



Contents lists available at ScienceDirect

Gondwana Research

journal homepage: www.elsevier.com/locate/gr

Periodicity of Karoo rift zone magmatism inferred from zircon ages of silicic rocks: Implications for the origin and environmental impact of the large igneous province

Arto Luttinen^{a,*}, Matti Kurhila^b, Riina Puttonen^c, Martin Whitehouse^d, Tom Andersen^{e,f}

^a Finnish Museum of Natural History, P.O. Box 44, 00014 University of Helsinki, Finland

^b Geological Survey of Finland, P.O. Box 77, 02151 Espoo, Finland

^c Vita Laboratoriot Oy, Laivakatu 5 F, 00150 Helsinki, Finland

^d Department of Geosciences, Swedish Museum of Natural History, P.O. Box 50007, 10405 Stockholm, Sweden

^e Department of Geosciences, University of Oslo, P.O. Box 1047, N-0316 Oslo, Norway

^f Department of Geology, University of Johannesburg, PO Box 524 Auckland Park, 2006 Johannesburg, South Africa

ARTICLE INFO

Article history:

Received 26 May 2021

Revised 7 February 2022

Accepted 12 March 2022

Available online 16 March 2022

Handling Editor: F. Pirajno

Keywords:

U-Pb dating

Hf isotopes

Flood basalt

Degassing

Mozambique

Southern Africa

ABSTRACT

New U-Pb ages for zircons constrain the duration of silicic magmatism and timing of coeval mafic magmatism across the main rift zone of the Karoo large igneous province in Mozambique. Our 190 ± 2 Ma, 188.4 ± 0.9 Ma, 181.7 ± 1.0 Ma, 180 ± 3 Ma, 178 ± 2 Ma and 172 ± 2 Ma ages support periodicity of Karoo magmatism previously inferred from $^{40}\text{Ar}/^{39}\text{Ar}$ age data. The ~ 190 – 188 Ma ages confirm early onset of magmatism and the ~ 182 – 178 Ma ages correlate the bimodal volcanic successions of the Lower Zambesi and the Movenne Formation with widespread silicic magmatism across the rift zone. The ~ 172 Ma age corresponds to waning magmatic activity. The age range and Hf isotopic compositions of zircons indicate up to ~ 9 Ma lifespan for the Jurassic silicic magma chambers and suggest that the ~ 2700 – 400 Ma xenocrysts represent crustal sources of the host rocks. The available chronological data indicate that the ~ 183 Ma main phase magmatism was largely confined within the main Karoo and Kalahari basins and that the preceding and subsequent phases were mainly associated with the Karoo rift zone. Judging from geochemical literature, different kinds of magmas were erupted during the successive magmatic phases. We calculate from published geochemical data that the mafic main phase magmas were relatively poor in CO_2 and SO_2 and the lava stacking patterns point to low eruption rates, which suggests that degassing of sedimentary wall-rocks of intrusions probably triggered the coeval Pliensbachian–Toarcian extinction. In contrast, the mafic late phase magmas were rich in CO_2 and SO_2 and at least some of the lavas indicate high eruption rates. We propose that efficient degassing from widespread mafic magmatism and explosive eruption of over $30,000 \text{ km}^3$ of silicic magmas in the Karoo rift zone linked the ~ 182 – 178 Ma late phase magmatism with contemporaneous global biosphere crises.

© 2022 The Authors. Published by Elsevier B.V. on behalf of International Association for Gondwana Research. This is an open access article under the CC BY license (<http://creativecommons.org/licenses/by/4.0/>).

1. Introduction

Many large igneous provinces (LIPs) show geochemical, geophysical, and structural evidence of heterogeneous mantle sources and complex feeder systems and magmatic development (e.g. Columbia River Basalt Group, Ethiopian Traps, Paraná; Garland et al., 1996; Pik et al., 1999; Camp and Hanan, 2008). Comprehensive chronological data are critical to understanding their origin,

evolution, and environmental influences (e.g. Kasbohm et al., 2021). The Early to Middle Jurassic rocks of the Karoo and Ferrar LIPs represent a vast magma system that formed along the paleo-Pacific margin of Gondwana before the breakup of the supercontinent (Fig. 1). High-precision isotope-dilution thermal ionization mass-spectrometry (ID-TIMS) U-Pb zircon and baddeleyite single grain ages indicate rapid emplacement of thick low-Ti dolerite sills across the main Karoo Basin, along the Transantarctic Mountains, and in Tasmania at ~ 183 – 182 Ma, and prove that a sizeable peak of magmatism coincided with the Pliensbachian–Toarcian

* Corresponding author.

E-mail address: arto.luttinen@helsinki.fi (A. Luttinen).

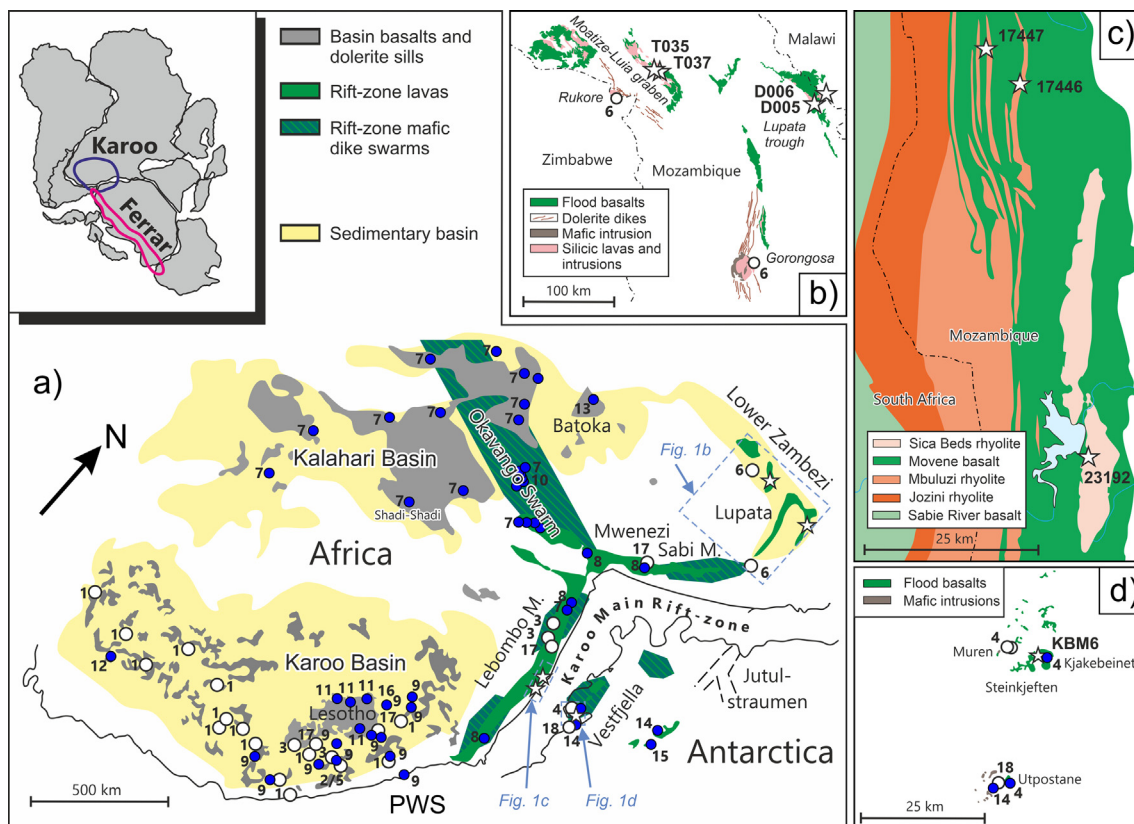


Fig. 1. U-Pb and $^{40}\text{Ar}/^{39}\text{Ar}$ ages in the Karoo large igneous province. Previous U-Pb and $^{40}\text{Ar}/^{39}\text{Ar}$ plagioclase plateau dating localities are indicated by white and blue circles, respectively, and new U-Pb dating localities by white stars. (a) Seaward-dipping volcanic successions, coast-parallel dike swarms, the Okavango dike swarm, and the Lower Zambezi comprise the Karoo rift zone (Burke and Dewey, 1973). (b) Karoo rock types and U-Pb age locations in northwestern Mozambique. (c) Karoo rock types and U-Pb age locations in southern Mozambique. (d) Karoo rock types and U-Pb and $^{40}\text{Ar}/^{39}\text{Ar}$ age locations in southern Vestfjella, Antarctica. PWS is proto-Weddell Sea basin. Age determinations: 1- Svensen et al., 2007; 2012; 2- Encarnacion et al., 1996; 3- Sell et al., 2014; 4- Luttinen et al., 2015; 5- Burgess et al., 2015; 6- Mänttari, 2008; 7-11- Jourdan et al., 2004, 2005, 2007b, c, 2008; 12- Ware et al., 2018; 13- Jones et al., 2001; 14- Zhang et al., 2003; 15- Luttinen, 2021; 16- Moulin et al., 2017; 17- Greber et al., 2020; 18 - Vuori, 2004.

mass-extinction (Svensen et al., 2012; Sell et al., 2014; Burgess et al., 2015; Ivanov et al., 2017; Greber et al., 2020).

However, most of the mafic and ultramafic rock types of the Karoo LIP are rapidly cooled basalt lavas and dikes that lack zircon and baddeleyite suitable for U-Pb dating. Consequently, the dataset of $^{40}\text{Ar}/^{39}\text{Ar}$ plagioclase plateau ages is regionally and geochemically more representative (Fig. 1). Comparison between the U-Pb ages and the $^{40}\text{Ar}/^{39}\text{Ar}$ ages (section 5) shows that, on one hand, the lavas of the Lesotho Formation, the main Karoo Basin, can be readily correlated with the geochemically similar ~ 183 – 182 Ma dolerite sills (Jourdan et al., 2007b; Moulin et al., 2017; Ware et al., 2018; Neumann et al., 2011; Galerne and Neumann, 2014), but, on the other hand, the range of $^{40}\text{Ar}/^{39}\text{Ar}$ ages (~ 190 – 174 Ma; e.g., Jourdan et al., 2004, 2005, 2007b, 2008; Luttinen et al., 2015; Moulin et al., 2017) suggests magmatism continued after and, in some places, significantly predated the ~ 183 Ma climax. Specifically, Jourdan et al. (2005) have proposed an episodic magma emplacement history for the Karoo LIP and Moulin et al. (2017) associated four magmatic phases at ~ 190 Ma, ~ 183 Ma, ~ 181 Ma, and ~ 178 – 174 Ma with recurrent Pliensbachian and Toarchian climate and biodiversity fluctuations (e.g. Korte and Hesselbo, 2011; Caruthers et al., 2013).

When evaluating the age data for Karoo magmatism, it is important to keep in mind that the geochronological (e.g. Jourdan et al., 2007b; Luttinen et al., 2015) and paleomagnetic (e.g. Hargraves et al., 1997) evidence for long-lived ~ 190 – 174 Ma igneous activity mainly comes from the main Karoo rift zone, i.e. the conjugate African and Antarctic rifted margins and the

associated failed rift arms, the Okavango dike swarm and the Lower Zambezi Basin (Burke and Dewey, 1973; Reeves, 1978; Jourdan et al., 2006) (Fig. 1). The up to nine kilometer thickness of the preserved strata (e.g. Hjellev and Winsnes, 1972; Luttinen and Furnes, 2000; Klausen, 2009), and results of thermochronology (Sirevaag et al., 2018) and the recognition of the magnetically defined dipping reflectors of the Antarctic rifted margins as Karoo flood basalts (Jokat et al., 2003), indicate that the Karoo rift zone was a volumetrically non-trivial part of the Karoo LIP (White, 1997). Numerous studies have concluded that the geochemically diverse igneous rock types of this rift structure and the notably geochemically uniform low-Ti tholeiites of the main Karoo and Kalahari basins represent genetically different subprovinces of the Karoo LIP. Given that these subprovinces were generated in diverse tectonic settings and were derived from contrasting mantle sources (Duncan et al., 1984; Marsh et al., 1997; Jourdan et al., 2007a; Luttinen et al., 2010; Ellam, 2006; Heinonen et al., 2010b; Harris et al., 2015; Luttinen, 2018; Turunen et al., 2019), neither age results nor genetic models should be applied across all parts of the Karoo LIP. The contrasting views of rapid versus prolonged and possibly episodic magmatism and the roles of different mantle sources represent a critical controversy in the assessment of the dynamic evolution of the Karoo LIP and its environmental impacts (Jourdan et al., 2005; Svensen et al., 2012; Ivanov et al., 2017; Moulin et al., 2017).

Here we report the first reliable age data for Karoo volcanism in Mozambique. Our study correlates Karoo rift zone magmatism in Mozambique with igneous activity elsewhere in the Karoo LIP by

U-Pb dating of zircons in silicic rocks and evaluates the relationships of the dated zircons and the magma sources using Lu-Hf isotopes. The great spread of ~190–172 Ma ages supports periodicity of Karoo magmatism previously inferred from $^{40}\text{Ar}/^{39}\text{Ar}$ age data. Published geochemical data indicate the parental magmas and the flux of magmatic volatiles varied considerably during different periods of volcanism.

2. Silicic rocks of the Karoo LIP

Silicic igneous rocks make up ~1 vol% of the Karoo LIP (Cleverly et al., 1984; White, 1997). Their occurrences are effectively confined to the African (Eales et al., 1984) and Antarctic rifted margins (Harris and Grantham, 1993; Harris et al., 2002; Vuori and Luttinen, 2003) where they comprise a significant component of the bimodal rift zone succession (Cleverly et al., 1984; Manninen et al., 2008; Melluso et al., 2008) (Supplementary Data S1), and mainly represent extrusive units at relatively high stratigraphic position or relatively small intrusions. Most of the silicic rocks are rhyolites, but the compositions range to dacitic types in most areas (Miller and Harris, 2007; Melluso et al., 2008; Manninen et al., 2008).

2.1. Lebombo monocline

The Lebombo monocline represents a seaward-dipping, north-south trending volcanic-intrusive succession which contains variably enriched low-Ti and high-Ti tholeiitic basalts and picrites, alkaline mafic rocks, and the main volume of silicic rocks associated with the Karoo LIP (Cleverly et al., 1984). The volume of the Lebombo rhyolites has been estimated to be at least 30,000 km³ (Cleverly et al., 1984). The Sabie River Basalt Formation, which dominates the basal part of the lava pile across most of the monocline, is overlain by a widespread and thick suite of rhyolitic and minor dacitic rocks that constitute the Jozini Formation (Miller and Harris, 2007). In the central part of the monocline, the Jozini rhyolites give way to the rhyolitic and minor dacitic rocks of the Mbuluzi Formation (Melluso et al., 2008; Manninen et al., 2008; Fig. 1). The uppermost units of the Mbuluzi Formation are interbedded with mafic lavas belonging to the capping Moveene Formation (Miller and Harris, 2007). The Jozini and Mbuluzi rhyolites are composed of numerous up to 200 m thick cooling units which mainly represent variably welded ash-flow tuffs (Cleverly et al., 1984; Manninen et al., 2008).

A distinctive rhyolite ridge, the Sica Beds (Pequenos Limpopos), overlies the Moveene mafic lavas and is the youngest preserved silicic unit of the Lebombo monocline (Melluso et al., 2008). An underlying hydrothermally altered paleo-laterite implies a considerable hiatus may coincide with the basalt-rhyolite contact (Manninen et al., 2008). The Sica Beds include variable types of rhyolites and the up to 100–150 m thick cooling units show typical features of densely welded ash-flow tuffs (Manninen et al., 2008). Additionally, minor rhyolitic units are found as intercalations within the Sabie River Basalt Formation (Olifants Beds, Twin Ridge Beds, Mkutshane Beds, Coeayana Beds, and several intrusive granophyre sheets; Eales et al., 1984). Several minor silicic intrusive and extrusive units are also found in the Mwenezi triple junction area, at the intersection of the Lebombo and Sabie monoclines (Fig. 1).

The eruption age of the Jozini rhyolites has been established at ~180 Ma (180.42 ± 0.47 Ma U-Pb ID-TIMS age for a chemically abraded single zircon grain by Greber et al., 2020; 179.6 ± 0.7 Ma $^{40}\text{Ar}/^{39}\text{Ar}$ age by Jourdan et al., 2007b). Additionally, a large granophyre sill at the contact of the Sabie River Basalt Formation and the Jozini Formation and a rhyolite boulder from a broadly similar stratigraphic position have yielded ID-TIMS U-Pb ages for

chemically abraded single zircons, respectively, from ~183 to 181 Ma and ~181 to 179 Ma (Sell et al., 2014). The authors interpreted the ages of the youngest zircons to date the emplacement of the granophyre at 181.31 ± 0.19 Ma and rhyolite at 179.3 ± 0.18 Ma. Furthermore, dating of zircons with the sensitive high-resolution ion microprobe (SHRIMP) yielded a U-Pb regression age of 180 ± 3 Ma for the Olifants Beds (Riley et al., 2004; Jourdan et al., 2005). Small silicic intrusions (granite, granophyre, syenite) in the Mwenezi triple junction area have been dated at 176.84 ± 0.06/0.2 Ma (U-Pb ID-TIMS; Greber et al., 2020) and ~178 Ma and ~176 Ma ($^{40}\text{Ar}/^{39}\text{Ar}$ hornblende and biotite ages; Jourdan et al., 2007b). The ages of the Mbuluzi and Sica Beds rhyolites have not been previously established.

2.2. Lower Zambezi – Lupata trough and Moatize-Luia graben

Silicic rock types have not been reported in the eastern part of the seaward-dipping Sabie monocline. In the very north-easternmost part of the Karoo rift zone, however, the Lupata trough and the Moatize-Luia graben areas are typified by bimodal volcanic and intrusive suites (Fig. 1b; Manninen et al., 2008). In the western part of the Moatize-Luia graben, thin rhyolitic to minor dacitic units are intercalated with mafic units and, in places, with lower-Karoo sandstones (Manninen et al., 2008). In the eastern part, extensive and thick rhyolites cap mafic lavas and dip 10–35° to southwest. The units typically represent variably welded ash-flow tuffs and include volcanic breccias, lapilli tuffs, and massive flow-banded lava-like rocks (Manninen et al., 2008). Some of the massive units probably represent lava flows and some may be subvolcanic intrusions. In the Lupata trough, the horseshoe-like exposure of Karoo volcanic rocks also records compositional bimodality. In the southwestern part of the trough, silicic rocks form a north-trending ridge over 30 km long and up to 4 km wide (Fig. 1b; Manninen et al., 2008). The eastward dipping rhyolites comprise a silicic interbed between mafic lavas. The silicic rocks typically are massive, but, in places, the thick units record flow-banding and brecciated structures. Silicic units also occur together with mafic lavas along the eastern flank of the Lupata trough, but the stratigraphy is not defined in detail. Our field observations suggest the silicic units form relatively thin intercalations within a predominantly mafic volcanic succession.

Two bimodal intrusive complexes are associated with the Karoo volcanic rocks in the area. The Rukore Intrusive Suite at the southern border of the Moatize-Luia graben (Fig. 1b) is mainly composed of quartz and feldspar porphyritic microgranite (Barton et al., 1991; Manninen et al., 2008). Between the Lupata trough and eastern Sabie monocline, the Gorongosa Intrusive Suite is dominated by a core of medium-grained alkali-feldspar granite-syenite which shows intrusive relation to the enclosing gabbro body (Manninen et al., 2008) (Fig. 1b). Both intrusive suites are associated with bimodal dolerite and quartz-feldspar porphyry dike swarms (Manninen et al., 2008).

The volcanic rocks of the Lupata and Moatize-Luia have not been previously dated. Mänttari (2008) reported a U-Pb ID-TIMS zircon concordia age of 181 ± 1 Ma for a syenite from the Gorongosa intrusive suite and constrained the age of the Rukore granite intrusion in the Moatize-Luia graben to be within 195–180 Ma.

2.3. Antarctic rifted margin

At the Antarctic margin, silicic Karoo extrusive rocks are not exposed. In the Jutulstraumen rift area, three small nepheline syenite and syenite plutons and geochemically similar dikes have been dated at 207–170 Ma using Rb-Sr whole rock and mineral, K-Ar whole rock, and $^{40}\text{Ar}/^{39}\text{Ar}$ hornblende, plagioclase, and whole rock methods (Allen, 1991; Grantham et al., 1998; Harris et al.,

2002; Curtis et al., 2008) (Fig. 1). Overall, the age data for these silicic intrusive rocks are inconclusive or inadequately documented, but they are compatible with onset of silicic magmatism well before the ~ 183 Ma main stage of Karoo magmatism (e.g. Curtis et al., 2008). In Vestfjella, at the conjugate margin of the Lebombo monocline, silicic rocks are rare. A ~ 2 m wide granite dike crosscuts the 182.2 ± 0.9 Ma West Muren gabbro dike ($^{206}\text{Pb}/^{238}\text{U}$ ID-TIMS, Luttinen et al., 2015) and several narrow silicic dikes crosscut the 181.2 ± 0.5 Ma Utpostane layered intrusion ($^{40}\text{Ar}/^{39}\text{Ar}$, Zhang et al., 2003; Vuori and Luttinen, 2003). An unpublished academic thesis included U-Pb ID-TIMS concordia ages of 181.1 ± 0.7 Ma and 180.0 ± 0.9 Ma for two zircon fractions from a granophyre dyke at Utpostane (Vuori, 2004). Additionally, another academic thesis (Romu, 2019) reports a $^{206}\text{Pb}/^{238}\text{U}$ SIMS zircon age of 165 ± 1 Ma for a Jurassic granite xenolith in one of the ~ 162 Ma ($^{40}\text{Ar}/^{39}\text{Ar}$ phlogopite, Luttinen et al., 2002) ultrapotassic lamproite dikes of southern Vestfjella.

3. Rationale, samples, and methods

3.1. Rationale

The great majority of Karoo mafic igneous rocks lack zircon and baddeleyite suitable for U-Pb dating due to rapid cooling. Furthermore, subsolidus alteration hampers $^{40}\text{Ar}/^{39}\text{Ar}$ plagioclase dating of the extrusive and intrusive mafic rocks of the main-rift zone as the predominance of relatively thin and vesicular lava flow units and the high abundance of cross-cutting dikes have promoted circulation of hydrothermal fluids. Previous geochronological studies have also shown that even visually unaltered plagioclase phenocrysts frequently have disturbed Ar-spectra due to excess ^{40}Ar , ^{40}Ar -loss, ^{39}Ar -recoil, and, possibly, due to secondary K-bearing micropores (e.g. Zhang et al., 2003; Luttinen et al., 2015).

Silicic interbeds between flood basalt lavas allow U-Pb zircon dating of the lava successions. Furthermore, the generation of silicic melts in within-plate settings is very likely triggered by intrusion of mantle-sourced magmas into the crust (e.g. Huppert and Sparks, 1988; Bryan and Ferrari, 2013), which means that age data for silicic rocks can be used to identify periods of mantle as well as crustal melting. However, numerous studies have demonstrated that zircons formed in silicic magma systems frequently record long and complex histories. For example, crystallization age ranges of up to ~ 9 Ma have been reported for silicic rocks due to incorporation of zircon antecrysts from previously formed parts of long-lived plumbing systems into moving magmas (e.g. Frazer et al., 2014). Moreover, zircon populations in silicic volcanic rocks may be dominated by inherited grains due to dissolution of liquidus zircons during thermal rejuvenation of crystal mush prior to major eruptions (Miller et al., 2007), and zircon xenocrysts derived from crustal magma sources and wall-rocks are likely to survive in silicic magma chambers. Pyroclastic units also tend to sample mixed zircon populations. Our aim is to constrain the ages and duration of magmatic activity in the Karoo rift zone using zircons from silicic rocks and cast light on the sources of silicic magmas. We have studied the Karoo silicic rocks using in situ U-Pb dating that helps to avoid analysis of metamict material and inclusions and facilitates representative sampling of complex zircon populations typical of silicic igneous rocks. In situ Lu-Hf isotopic analyses provide valuable information on compositional variability of the dated crystals and the sources of the silicic parental magmas.

3.2. Samples

Our samples belong to the collection of the Finnish Museum of Natural History and they were collected by the first author during

field campaigns in 1998 (Antarctica), 2006 (Lebombo), and 2012 (Lower Zambezi). The sample locations are illustrated in Fig. 1 and detailed descriptions of petrographic features and studied zircons are reported in Supplementary Data S1.

3.2.1. Lebombo monocline – Mbuluzi rhyolites and Sica beds

Our samples of the Mbuluzi Formation represent two silicic units intercalated with basalts close to the base of the Movene Formation (Fig. 1c). Samples 17446 and 17447 are vitrophyric rhyolites that may well represent rheomorphic lava (cf. Miller and Harris, 2007). Sample 17447 is stratigraphically older (Fig. 1c). Sample 23192A from the Sica Beds is vitrophyric rhyolite that probably represents rheomorphic lava. The Mbuluzi and Sica Beds rhyolites have small, prismatic, mostly elongate but in some cases stubby zircons. The zircons are quite homogeneous in backscattered electron images, but a cathodoluminescence image of sample 17446 reveals that the grains with lower U and Pb contents typically are internally homogeneous, whereas the grains with higher U and Pb contents exhibit well-developed zoning.

3.2.2. Lower Zambezi – Lupata and Moatize-Luia rhyolites

Samples D005B, D006B, T035, and T037 (AL-D005B-12, AL-D006B-12, AL-T035-12, AL-T037-12) represent silicic rocks of the Lupata trough and the Moatize-Luia graben in the Lower Zambezi (Fig. 1a, b). Samples D005B from the Luenha trough and T037 from the Moatize-Luia graben are pyroclastic rocks and we interpret them to be lithic tuffs. Sample D005B represents the interior of a > 5 m thick silicic unit, whereas sample T037 is a lithic tuff collected from a field of ~ 1 m silicic boulders. The lithic tuffs are characterized by colorless, transparent, prismatic but variably broken low-U zircons that are fractured and contain variable amounts of inclusions. Zircons in sample D005b typically are stubby and homogeneous. In the case of sample T037, many of the zircon grains are fractured and contain many inclusions. Zoning is vague and irregular. Sample T035 represents ~ 2 m boulder of a sanidine porphyritic massive rhyolite on the apron of a rhyolite ridge. Sample T035 has mainly zircons that are colorless and mostly prismatic, but many of the grains are fragments. Dark inclusions are rare. The analyzed grains are intensely cracked and often display oscillatory or sector zoning. Sample D006B is a peperite-type composite of volcanic rock fragments within silty matrix. The lava fragments are opaque vitrophyric, vesicular rhyolite. The peperite unit has a notably heterogeneous zircon population of prismatic and anhedral grains. The grains can be divided into a colorless transparent type, a light brown transparent type, and a brown cloudy type. They frequently are altered and show variable zoning and core-rim structures.

3.2.3. Antarctic margin – Granite xenolith in lamproite dike

A small suite of ~ 162 Ma lamproite dikes cuts through the flood basalt lava succession in the Kjakebeinet area, southern Vestfjella (Luttinen et al., 2002). Some of the dikes contain abundant xenoliths that represent diverse crustal rock types. Most of the xenoliths are 1.3–1.1 Ga granitoids which can be correlated with the Precambrian basement of western Dronning Maud Land, Antarctica (Romu, 2019). Sample KBM6 (AL-KBM6-98) is fine-grained and equigranular granite xenolith. The granite xenolith has fairly large (>300 μm), euhedral, stubby low-U zircons. We included sample KBM6 in our study for the purpose of Hf isotopic analyses. In addition to new Lu-Hf data, we present a re-interpretation of the U-Pb results originally reported by Romu (2019).

3.3. U-Pb dating

The SIMS analyses were performed at the NordSIM laboratory, Swedish Museum of Natural History, Stockholm. We processed 2–3 kg of each sample in a jaw crusher and ground the chips into grain size of < 350 µm using a swing mill. In order to avoid excessive pulverization, we only used the outer grindstone in the swing mill and kept the run times within about thirty seconds. Fine dust was removed using a sieve and, finally, by careful washing of the zircon-bearing fraction. The heavy minerals were further extracted with di-iodomethane ($d \sim 3.3 \text{ g/cm}^3$) and divided into magnetic and non-magnetic fractions with a Frantz isodynamic magnetic separator using 1.4 A current with a slope of 8° and a tilt of 4°. The recovered non-magnetic fraction was then separated using a series of Clerici's solution up to 4.3 g/cm³ in order to obtain zircon concentrates.

A range of zircon crystals, representative of the whole sample, was selected under the microscope and mounted in epoxy, polished, and gold-coated. Backscattered electron images were taken of the mount surface and the selection of the zircon crystals to be dated was mainly based on the textures seen on these images (Supplementary Data S1). Cathodoluminescence imaging was limited to samples 17,446 and KBM6 (Supplementary Data S1) due to potential detachment of small zircons from the mount under the required high acceleration voltage. The ion microprobe analyses were performed using Cameca IMS 1270 and Cameca IMS 1280 instruments during three analytical sessions. The spot diameter for the primary O²⁻ ion beam (nominal beam current 5nA) was ~ 25 µm and oxygen flooding in the sample chamber was used to increase the production of Pb⁺ ions. Three or four counting blocks, each including four cycles of the Zr, Hf, Pb, Th, and U species of interest, were measured from each spot. The mass resolution (M/ΔM) was 5300 (10%).

The data were calibrated against a zircon standard 91500 (1065 Ma; Wiedenbeck et al., 1995) and corrected for modern common-Pb (T = 0; Stacey and Kramers, 1975). The procedure was essentially similar to that described in detail by Whitehouse et al. (1999) and Whitehouse and Kamber (2005). Plotting and calculation of the weighted average ages were done with the Isoplot 4.15 Excel Add-in (Ludwig, 2012). All uncertainties are plotted and the calculated age errors are reported at 2σ level, unless otherwise indicated. Decay constant errors are ignored.

Because the U-contents of many zircon grains are low, especially in the Lebombo samples, and due to the young ages of these rocks, extremely low Pb count rates proved to be somewhat problematic. As the low Pb concentrations often lead to common-Pb overcorrection (because of Hg interference and the assumed modern origin of the common Pb), we prefer the 207-corrected ²⁰⁶Pb/²³⁸U ages for SIMS data. Here, the age is the concordia intercept of a line passing through an assumed common-Pb isotopic composition of the common-Pb (Stacey and Kramers, 1975) and the measured ²³⁸U/²⁰⁶Pb ratio on a Tera-Wasserburg diagram. With this approach, we can utilize also those measurements where the corrected signal of ²⁰⁷Pb did not exceed the background. For comparison, we also calculated the concordia ages with uncorrected ²⁰⁶Pb/²³⁸U and ²⁰⁷Pb/²⁰⁶Pb ratios, when possible.

We rejected data points that have an extremely high common-Pb (²⁰⁶Pb/²⁰⁴Pb < 100). Because of the very low overall Pb concentrations of many zircon grains, we did not want to employ a stricter cut-off value. Those points that have discordance of > 10% (to closest 1σ limit), calculated from uncorrected ²⁰⁷Pb/²³⁵U and ²⁰⁶Pb/²³⁸U ratios, were excluded from the age calculations. When errors for ²⁰⁷Pb/²³⁵U ratios were unavailable, an alternative discordance check using the ²⁰⁶Pb/²³⁸U and ²⁰⁷Pb/²⁰⁶Pb ratios was performed. Usually, ²⁰⁷Pb/²⁰⁶Pb ages are only used for discordance calculations of Precambrian ages, because the ²⁰⁷Pb/²⁰⁶Pb age

becomes very imprecise towards younger ages. When the results were discordant even with the huge range of the ²⁰⁷Pb/²⁰⁶Pb ages, we considered those data as meaningless and rejected them.

3.4. Lu-Hf isotopic analysis

The Lu–Hf analyses were performed with a NU Plasma HR multicollector inductively coupled plasma source mass spectrometer and a Cetac LS213G2 + Nd:YAG 213 nm laser microprobe at the Department of Geosciences, University of Oslo. For information on the analytical protocols, the reader is referred to Elburg et al. (2013). Interference from ¹⁷⁶Yb on mass 176 was corrected using the measured signal on mass 172 (interference-free ¹⁷²Yb) and mass discrimination factors for Yb determined from measurement of ¹⁷⁴Yb/¹⁷²Yb ratio, after correction for interference from ¹⁷⁴Hf. Interference from ¹⁷⁶Lu was corrected from observed ¹⁷⁵Lu, using mass discrimination factor of Hf as a proxy.

The long-term precision based on reference zircons run as unknowns (errors quoted at the 2-sigma level) is as follows. *Mud Tank*: ¹⁷⁶Hf/¹⁷⁷Hf = 0.282504 ± 0.000040 (published value: 0.282507, Woodhead and Hergt, 2005), ¹⁷⁸Hf/¹⁷⁷Hf = 1.46725 ± 0.00012, n = 1598; *Temora 2*: ¹⁷⁶Hf/¹⁷⁷Hf = 0.282680 ± 0.000042 (published value: 0.282686, Woodhead and Hergt, 2005), ¹⁷⁸Hf/¹⁷⁷Hf = 1.46726 ± 0.00009, n = 51 (initial ¹⁷⁶Hf/¹⁷⁷Hf at 417 Ma: 0.282672 ± 0.000042); *LV11*: ¹⁷⁶Hf/¹⁷⁷Hf = 0.282828 ± 0.000071 (published solution analysis: 0.282830 ± 0.000028, Heinonen et al., 2010a), ¹⁷⁸Hf/¹⁷⁷Hf = 1.46723 ± 0.00011, n = 921 (initial ¹⁷⁶Hf/¹⁷⁷Hf at 290 Ma: 0.282812 ± 0.000071). The ε_{Hf} values were calculated using λ_{176Lu} = 1.867·10⁻¹¹ a⁻¹ (Söderlund et al., 2004) and CHUR and Depleted Mantle models of Bouvier et al. (2008) and Griffin et al. (2000, modified to the parameters used), respectively. We targeted dated parts of zircons in the Hf isotopic analyses, but, in the case of small crystals, the compositional data effectively corresponds to the bulk composition of the dated zircon grains due to the large (~60 µm) diameter of the laser beam.

4. Results

The U-Pb age and Lu-Hf isotopic results illustrated in Figs. 2–3 and Supplementary Data S2, and full data are listed in Supplementary Data S3–S4.

4.1. U-Pb ages

The U-Pb data are listed in Supplementary Data S3. Discordant (>10%) and high common-Pb results were not included in the calculation of 207-corrected ²⁰⁶Pb/²³⁸U ages and are excluded from the results and discussion. Summarizing, the Jurassic ages of individual zircons range from ~ 195 Ma to ~ 160 Ma and the concordia ages and weighted average ²⁰⁶Pb/²³⁸U ages of samples typically coincide (Fig. 2 and Supplementary Data S2). Several samples contain inherited ~ 2722 Ma (²⁰⁷Pb/²⁰⁶Pb age) to ~ 381 Ma pre-Jurassic zircons that can be correlated with Archean to Paleozoic basements of the Kalahari-Kaapvaal craton and adjacent mobile belts (Fig. 3).

In the lithic tuff D005b (Lower Zambezi), the zircons yield a weighted average age and 2σ error of 181.7 ± 1.0 Ma (Fig. 2a). One ~ 190 Ma grain was excluded from the average. In the rhyolite lava T035 (Lower Zambezi), the zircons yield an age of 188.4 ± 0.9 Ma (Fig. 2c), whereas the rhyolite 17447 (Lebombo monocline) has a weighted average age of 178 ± 2 Ma (Fig. 2f) and zircons in the rhyolite 23192A (Lebombo monocline) provide an age of 172 ± 2 Ma (Fig. 2g). The Antarctic granite xenolith KBM6 has two inherited ~ 469 Ma and ~ 1100 Ma grains, whereas the Jurassic grains give an age of 165.0 ± 0.9 Ma (²⁰⁶Pb/²³⁸U age recalculated

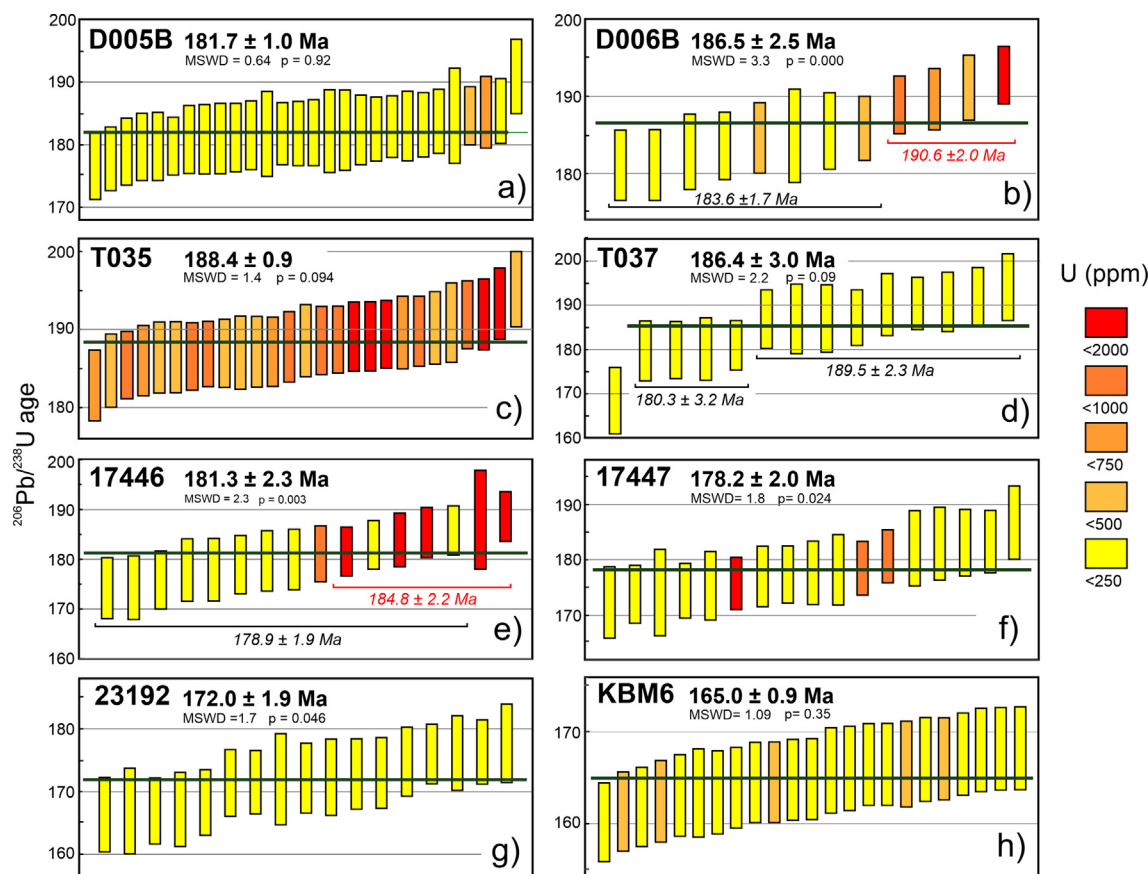


Fig. 2. Concordant 207-corrected $^{206}\text{Pb}/^{238}\text{U}$ SIMS ages for silicic rocks of the Karoo rift zone. Color coding refers to U-contents. The ages of relatively U-rich (>400 ppm in b; >750 ppm in e) and U-poor zircons are shown with red. The ages of relatively old and young zircons (the youngest ~ 168 Ma grain excluded; see text) are separately indicated in d). Age error corresponds to 2σ (decay constant errors are ignored).

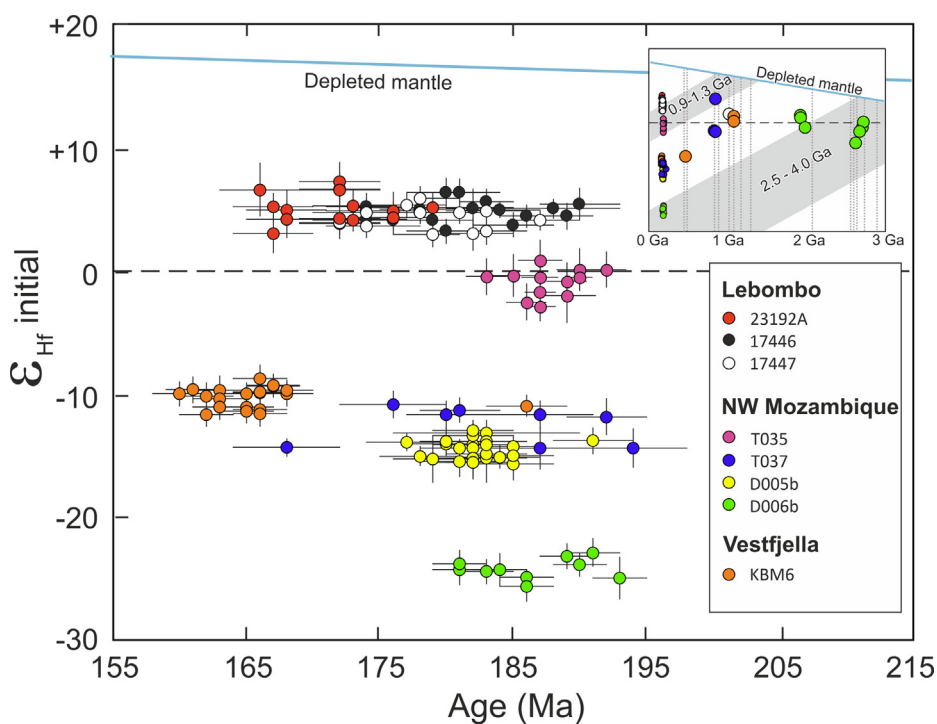


Fig. 3. ϵ_{Hf} vs. age diagram for zircons in silicic extrusive and intrusive rocks from the Karoo rift zone. The inset shows results for inherited zircons with the U-Pb zircon TIMS ages of basement rocks in northwest Mozambique (vertical lines; Mänttär, 2008) and Hf isotopic evolution of depleted mantle (Griffin et al., 2000) and evolution paths for 4.0–2.5 Ga and 1.3–0.9 Ga crust indicated (shaded bands; $^{176}\text{Lu}/^{177}\text{Hf} = 0.015$; Griffin et al., 2004).

from Romu, 2019; Fig. 2h). One of the ~ 165 Ma grains has a ~ 186 Ma old core that was excluded from the average.

The tuff sample T037 and peperite sample D006b (Lower Zambezi), and the rhyolite sample 17446 (Lebombo monocline) have more complex zircon age distributions. The Mbuluzi rhyolite 17446 contains one inherited ~ 1021 Ma zircon and the ages of the Jurassic grains average 181 ± 2 Ma, i.e. marginally older than that of the stratigraphically older rhyolite 17447 (Fig. 1c). Five grains can be distinguished by their higher U contents, however. The more U-rich zircons (872–2606 ppm) provide an older average age of 185 ± 2 Ma, whereas the U-poor zircons (<150 ppm) yield an average age of 179 ± 2 Ma that overlaps with the age of the underlying rhyolite 17447 (Fig. 2g). In the Lupata peperite sample D006b, nine grains are inherited, probably represent the silty matrix, and have Precambrian $^{207}\text{Pb}/^{206}\text{Pb}$ ages from ~ 2722 Ma to ~ 1922 Ma. The Jurassic zircons have an average age of 187 ± 3 Ma, but, as in the case of sample 17446, the relatively U-rich grains (437–1776 ppm) provide an older average age of 191 ± 2 Ma than the U-poor grains (70–272 ppm) which are dated at 184 ± 2 Ma (Fig. 2b). Finally, in the Moatize-Luia tuff T037, ten inherited ~ 906 Ma to ~ 381 Ma grains and one exceptionally young ~ 168 Ma grain were excluded from the average age of 186 ± 3 Ma. The age results show evidence of bimodality (Supplementary Data S2) and the four youngest grains (168 Ma grain excluded) have an age of 180 ± 3 Ma and the nine oldest grains are dated at 190 ± 2 Ma (Fig. 2d).

4.2. Hf isotope data

Lu-Hf isotopic data for the zircons dated using SIMS are listed in Supplementary Data S4 and shown in an ε_{Hf} vs. age plot in Fig. 3. The initial Hf isotopic compositions are diverse, but individual samples have isotopically quite uniform Jurassic zircon populations. Zircons in the Lebombo monocline samples (17446, 17447, 23192A) have similar radiogenic ε_{Hf} of +3 to +7, apart from one anomalous grain in the Sica Beds sample ($\varepsilon_{\text{Hf}} + 15$; not shown in Fig. 3). Zircons in the Moatize-Luia graben and Lupata trough samples, Lower Zambezi, exhibit a range of ε_{Hf} from nearly chondritic (lava T035), through moderately unradiogenic (–11 to –16; lithic tuffs T037 and D005b) to strongly unradiogenic (–23 to –25; peperite D006b) values. The Antarctic xenolith (KBM6) has initial ε_{Hf} of –9 to –11. Crucially, none of the samples records correlation between initial ε_{Hf} and ages in the case of Jurassic zircons (Fig. 3).

The inherited pre-Jurassic zircons have nearly chondritic initial isotopic compositions ($\sim +6$ to -6) suggestive of significant juvenile crustal components and their ages coincide with the ages of regional rock types reported by Mänttari (2008) (Fig. 3).

5. Discussion

We focus our discussion on three general topics: First, we use our results to address the timing of magmatism and the sources of silicic magmas in the Mozambican parts of the Karoo LIP. Second, we review the chronological evidence for magmatism in the Karoo basins and rift zone. Third, building on the chronological, geochemical, petrological, and volcanological information, we assess the release of mantle-derived volatiles at different phases and in different regions of magmatic activity in the Karoo LIP. All cited $^{40}\text{Ar}/^{39}\text{Ar}$ ages are plagioclase plateau ages, unless otherwise indicated, and are expressed using the ^{40}K decay constants of Renne et al. (2011), which facilitates direct comparison with U-Pb age data. The errors are shown at 2-sigma level.

5.1. Crystallization ages and lifespan of silicic magma systems

The interpretation of our age data is complicated due to geological and methodological issues (see section 3.1.). The notable age dispersion of ~ 4 – 10 Ma in many of our samples, sometimes in different parts of single crystals, significantly exceeds the 1% reproducibility of the Temora standard at Nordsim. The mean square weighted deviation (MSWD) values are mainly outside the expected range of a single age population (Wendt and Carl, 1991), which suggests long crystallization history, reworking of the U-Pb system, or analytical bias, or a combination of these factors.

Most of our zircons are concordant and U-poor and the samples do not exhibit negatively skewed age distribution patterns (Supplementary Data S2) or negative correlation between ages and U-contents that would suggest significant Pb-loss (Spencer et al., 2016) (Fig. 4). Overall, we regard that the < 185 Ma average ages of U-poor zircons have not experienced Pb-loss and correspond to (possibly prolonged) periods of crystallization within silicic magma plumbing systems. We suspect, however, that the single ~ 168 Ma grain (sample T037), which records an anomalous young age among all zircons from the Lower Zambezi study area, has been affected by Pb-loss despite its low U content.

The > 185 Ma ages are more problematic. Williams and Hergt (2000) and White and Ireland (2012) among others have shown that ion probe dating of U-rich zircons may yield bias to old ages due to matrix effects and urged cautious interpretation of zircons with U contents of > 2000 ppm. None of our zircons has a U content of > 2000 ppm and in most of the grains it is < 1000 ppm. However, due to moderate positive correlation between the U contents and apparent ages in samples D006B ($r = 0.73$) and 17446 ($r = 0.65$), we suspect that the ages of the relatively U-rich grains are subject to matrix effects; therefore, in these samples only the U-poor grains provide reliable age data for zircon crystallization (Fig. 4). It is also possible to address the critical threshold of U contents that cause matrix effect using “displacement per atom” (D_{dpa}) values that provide a quantitative estimate of radiation damage in the zircon lattice (e.g. Ewing et al., 2003). Gao et al. (2014) examined the relationship between ages and calculated D_{dpa} values using published data on zircon standards and other zircons and proposed that matrix effects become significant at D_{dpa} values of > 0.08 . While our dataset is too heterogeneous for us to examine the correlation between ages and D_{dpa} values in detail, our Jurassic zircons have $D_{\text{dpa}} > 0.08$ at U contents of > 1000 ppm. It should be mentioned, therefore, that most of the > 185 Ma grains in D006B have < 1000 ppm of U. Moreover, the cathodoluminescence images reveal the U-rich grains in sample 17446 show marked zoning, whereas the U-poor grains do not (Supplementary Data S1). We consider that the apparent age differences in these samples could be real, but do not use age results from these samples in our geological interpretations.

It is worthwhile to point out that all of our samples from the Lower Zambezi yielded > 185 Ma old ages. The predominance of old grains in samples T035 and T037 cannot be readily ascribed to matrix effects: First, zircons in rhyolite T035 show poor correlation between ages and U contents ($r = 0.33$) and most of the zircons have U contents of < 1000 ppm. Given that the intercept from linear regression of U vs. age in Fig. 4 is as old as ~ 187 Ma, we consider that the weighted average age of 188.4 ± 0.9 Ma corresponds to the average zircon crystallization age in the magma chamber that fed rhyolite T035. Second, zircons in tuff T037 are U-poor and, therefore, their ages are not suspect of Pb-loss or matrix effects. We interpret the 186.4 ± 3.0 Ma age as the average zircon

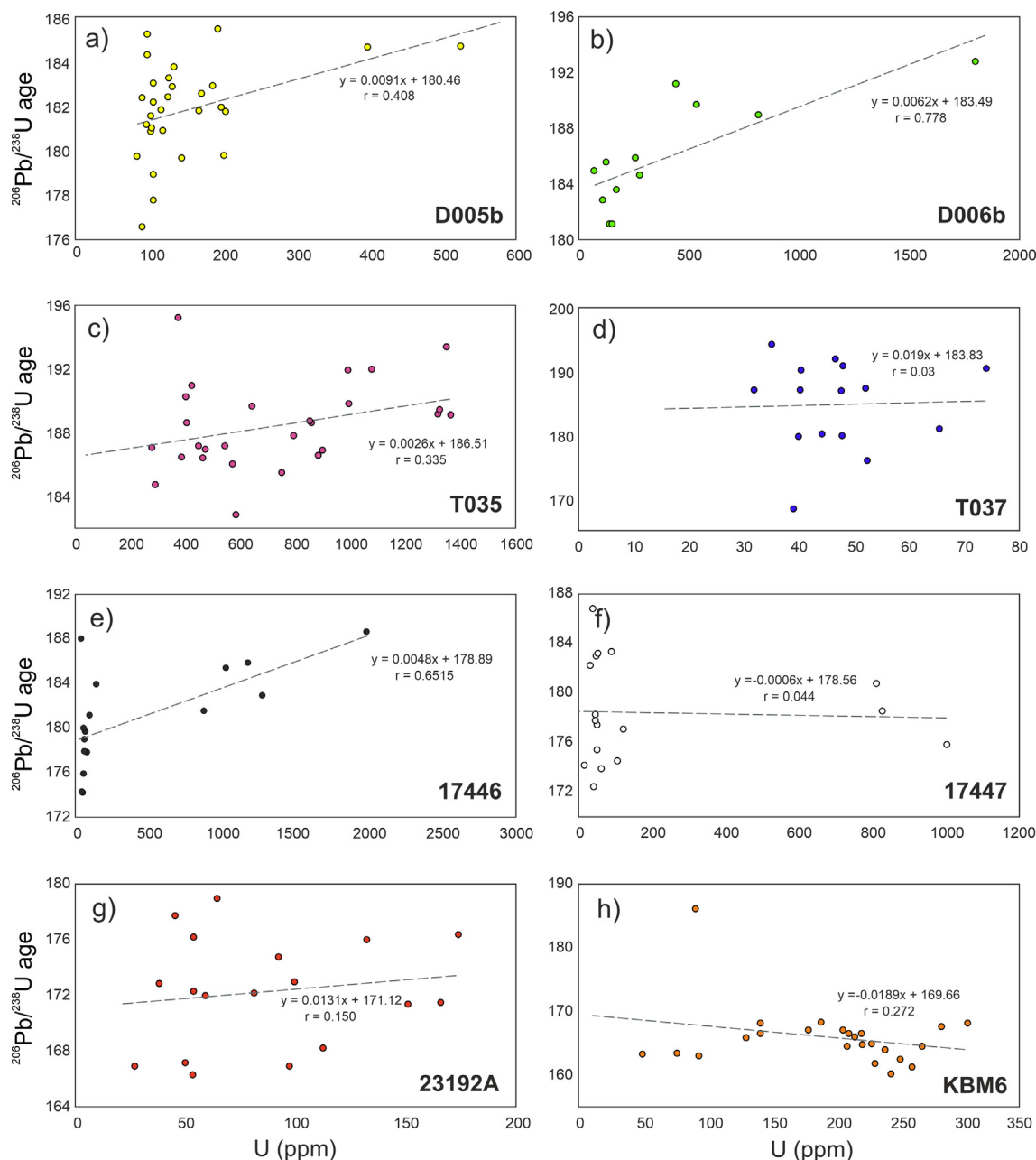


Fig. 4. $^{206}\text{Pb}/^{238}\text{U}$ ages vs. U concentration diagrams for analyzed zircons in the studied samples. Linear regression equations and correlation coefficients are indicated.

crystallization age in tuff T037, and we maintain that the age results for rhyolite T035 and tuff T037 prove crystallization of zircons in silicic magmas in the Lower Zambezi several millions of years before the ~ 183 Ma main pulse of Karoo magmatism.

The results from the Lower Zambezi samples show evidence for long-lasting silicic igneous activity and the bimodal age distribution is suggestive of two distinctive phases at ~ 190 – 188 Ma and ~ 182 – 180 Ma (Supplementary Data S2). We propose that the chemically and Hf isotopically similar 190 ± 2 Ma and 180 ± 3 Ma zircons in tuff T037 (Figs. 2–3) record formation and re-activation of a long-lived magma system. Sample D005B only has one ~ 190 Ma zircon, but the notably similar bimodal age distributions and Hf isotopic and chemical compositions in samples T037 and D005B (Figs. 2–4) suggest these tuffs may represent eruption of pyroclastic material from the same magma chamber.

The age results from the Lebombo monocline and Vestfjella are also suggestive of long-lived silicic magmatism, but the evidence is more ambiguous. First, the compositionally distinctive but Hf isotopically indistinctive ~ 185 Ma zircons in sample 17446 could reveal an initial phase in the magma source of the Mbuluzi rhyolites, Lebombo area, although the old ages of U-rich zircons are suspect of analytical bias. Second, we interpret the ~ 186 Ma core in one of the ~ 165 Ma grains to represent inheritance from earlier silicic magmatism in Vestfjella. We consider that the 165.0 ± 0.9 Ma average age of xenolith KBM6 coincides with the emplacement age of the sampled granite intrusion within error. Third, U-poor zircons in the Lebombo rhyolites 17447 and 23192B are unlikely to represent single age populations ($<5\%$ probability; Fig. 2) and we consider their respective 178 ± 2 Ma and 172 ± 2 Ma ages to record the average age of zircons formed in the magma chambers before the eruption of the dated volcanic units. However, the ages

would be just within the acceptable range of a single age population if the oldest grain is excluded from the average, and we interpret the average ages to correspond to the eruption ages of these units within error.

5.2. The crustal sources of silicic magmas

We envisage that the zircon ages from silicic rocks register periods of crustal melting and development of silicic magma systems in response to emplacement of mafic magmas (Huppert and Sparks, 1988). Judging from our U-Pb ages and Hf isotopic evidence for long-lived magma storage and transport systems in the Lower Zambezi, at least some of the silicic magmatism recorded rejuvenation of pre-existing magma chambers, possibly by coeval mafic magmas. Direct textural evidence of bimodality is recorded, for example, in the Jozini rhyolites (Misra et al., 2020) and the silicic volcanic and intrusive rocks in the Lower Zambezi (Manninen et al., 2008).

Previous studies have emphasized O, Sr, and Pb isotopic similarities between the silicic and mafic rock types of the Lebombo monocline and have ascribed the origin of the Jozini and Mbuluzi rhyolites to advanced fractional crystallization of mafic Karoo magmas (Melluso et al. 2008), or to partial melting of juvenile mafic crust formed by Karoo magmatism (Cleverly et al., 1984; Miller and Harris, 2007). In contrast, some of the stratigraphically older silicic units within the Sabie River Basalt Formation (e.g. Mkutshane Beds) have Sr and Pb isotopic compositions indicative of Precambrian crustal sources (Bristow et al., 1984; Cleverly et al., 1984). Recently, Greber et al. (2020) reported Hf isotopic data for two silicic units from the rift zone. The zircons in their Jozini rhyolite have mildly radiogenic initial Hf isotopic composition ($\epsilon_{\text{Hf}} + 4$ to $+ 2$) consistent with a juvenile crustal source. In contrast, the zircons in a Mwenezi syenite were highly unradiogenic ($\epsilon_{\text{Hf}} - 11$), but Greber et al. (2020) nevertheless favored a juvenile source similar to nearby Mwenezi picrites ($\epsilon_{\text{Hf}} - 10$; Kamenetsky et al., 2017). Our data indicate notable Hf isotopic variability in the silicic rocks. On one hand, the data for the Mbuluzi and Sica Beds rhyolites ($\epsilon_{\text{Hf}} + 7$ to $+ 2$; Fig. 3) add on to the previously established isotopic evidence that links the Lebombo monocline rhyolites to juvenile mafic crustal sources. On the other hand, our data on zircon xenocrysts reveal Hf isotopically suitable ~ 2.6 – 0.9 Ga crustal sources for most of the studied silicic rocks (ϵ_{Hf} at 180 Ma -37 to -4 assuming crustal $^{176}\text{Lu}/^{177}\text{Hf}$ of 0.015; Griffin et al., 2004; Fig. 3). We consider that, with the possible exception of the Lebombo samples, the silicic rocks in our study are likely to represent partial melting of Proterozoic to Archean crust. Significant melt contribution from the isotopically highly variable mafic rocks of the Karoo rift zone ($\epsilon_{\text{Hf}} + 5$ to -11 and $\epsilon_{\text{Nd}} + 9$ to $- 19$; e.g. Hawkesworth et al., 1984; Sweeney et al., 1994; Riley et al., 2005; Jourdan et al., 2007a; Kamenetsky et al., 2017) cannot be precluded based on just Hf isotopic compositions, but we point out that the mafic rocks probably derived their radiogenic Hf isotopic compositions from crustal wall-rocks during magma ascent (e.g. Neumann et al., 2011; Heinonen et al., 2016).

5.3. Chronology of Karoo magmatism in Mozambique

Karoo-related mafic and silicic rocks are widespread in Mozambique, but they represent one of the least-studied parts of the Karoo LIP. Our results provide the first reliable age data for Karoo-related silicic volcanic rocks in Mozambique and constrain the ages of the associated flood basalts.

In the Lebombo monocline area, the dated Mbuluzi and Sica Beds rhyolites represent, respectively, intercalations within and a capping unit atop of the basaltic Movene Formation. In the Mbuluzi sample 17447 and the Sica Beds sample 23192A, the zircon ages

are probably statistically indistinguishable from the eruption ages of these units. We regard that the basalts at the base of the Movene Formation erupted coevally with rhyolite 17447 at ~ 178 Ma and the occurrence of a paleolaterite underneath the ~ 172 Ma Sica Beds (Manninen et al., 2008) suggests to us that the Movene Formation as a whole probably formed within a short period of time. Previously, the Movene Formation has been considered to be significantly younger, possibly ~ 140 Ma (Watkeys, 2002), but our results show they formed shortly after the stratigraphically underlying ~ 180 – 179 Ma Jozini rhyolites (Jourdan et al., 2007b; Sell et al., 2014; Greber et al., 2020), which is consistent with the geochemical similarity between the Movene and Sabie River basalts (Manninen et al. 2008; Melluso et al., 2008). The mafic lavas which overlie the Sica Beds are poorly exposed and little-studied (Manninen et al., 2008), and, for example, the highly alkaline lavas may well represent the waning phase of Karoo magmatism or significantly younger evolutionary stages of the African rifted margin.

In the Lower Zambezi area, tuff D005B represents a silicic unit between mafic lavas of the Lupata trough (Fig. 1). The average 181.7 ± 1.0 Ma age of Hf-isotopically uniform zircons in tuff D005B probably corresponds to the eruption age of this unit and we interpret this as a feasible estimate of the eruption age of the Lupata bimodal volcanic succession. In the Moatize-Luia graben, detailed volcanic stratigraphy has not been established, but tuff T037 represents the silicic units that appear to cap the suite of mafic lavas that fill the graben structure (Manninen et al., 2008). We interpret the younger 180 ± 3 Ma population of four zircons in T037 to provide the minimum age and a plausible eruption age estimate for the mafic lavas in the Moatize-Luia graben. Previous U-Pb ID-TIMS zircon ages of 180.9 ± 0.6 Ma and 180.6 ± 0.6 Ma for the Gorongosa syenite intrusion ($^{206}\text{Pb}/^{238}\text{U}$ ages recalculated from Mänttari, 2008) suggest ~ 182 – 180 Ma silicic magmatism was widespread in the Lower Zambezi area (Fig. 1b).

We interpret the 188.4 ± 0.9 Ma age of rhyolite T035 to represent the formation age of the sampled unit within error. The stratigraphic position of the rhyolite is unknown, but we suspect it may represent one of the dikes associated with the nearby Rukore Intrusive Suite (Barton et al., 1991; Fig. 1b) for which ID-TIMS dating of two zircon fractions from a granite has yielded ages of 189 ± 1 Ma and 186 ± 1 Ma ($^{206}\text{Pb}/^{238}\text{U}$ ages recalculated from Mänttari, 2008). Our tuff sample T037, and possibly the peperite sample D006B, appear to register coeval early phase silicic magmatism in the Lower Zambezi, whereas possible mafic age-correlatives of the ~ 189 – 186 Ma silicic magmatism have not been reported in the Lower Zambezi area. However, preliminary $^{40}\text{Ar}/^{39}\text{Ar}$ age data suggest ~ 186 Ma mafic intrusive activity in the Gorongosa dike swarm (Fred Jourdan, personal communication, 2019). Overall, our results prove that (1) some of the earliest manifestations of Karoo-related magmatism took place in the Lower Zambezi region, (2) the exposed Lupata and Moatize-Luia rhyolites and the intercalated basalts are part of the Karoo LIP rather than correlatives of Cretaceous alkaline igneous rocks of southern Malawi (e.g. Eby et al., 1995), and (3) the silicic Mbuluzi Formation and mafic Movene Formation were formed within a few million years after the underlying volcanic units of the Lebombo monocline.

5.4. Chronology of Karoo magmatism

Here we examine previous and new age data and discuss the duration and periodicity of magmatism in the Karoo LIP using presently available concordant U-Pb and $^{40}\text{Ar}/^{39}\text{Ar}$ plagioclase plateau ages for different parts of the Karoo province (Figs. 5–6). These ages include results for two Antarctic samples from an unpublished PhD thesis (Vuori, 2004) and we provide the U-Pb ID-TIMS data in Supplementary Data S5 with the permission from the author.

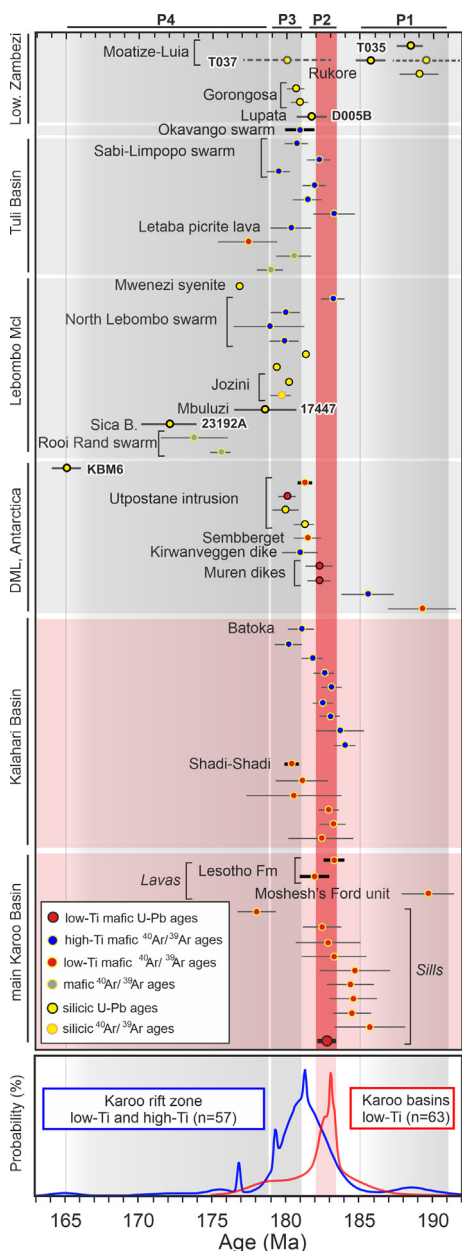


Fig. 5. Compiled U-Pb zircon ages and $^{40}\text{Ar}/^{39}\text{Ar}$ plagioclase plateau ages for the Karoo LIP. The age data are grouped on the basis of geographical and tectonic settings (i.e. Karoo-related basins vs. segments of Karoo rift zone) and the geochemical compositions are indicated (low-Ti mafic, high-Ti mafic, undefined mafic, silicic). Probability distribution plots for the low-Ti rocks of the Karoo basins and the low-Ti and high-Ti rocks of the Karoo rift zone are shown at the base. The ages of the studied samples (bold) and units mentioned in the text (e.g. the Okavango dike swarm, the Shadi-Shadi lava suite, and the Moshesh's Ford unit) are indicated. Ages with thick error bars are averages of several samples (see section 5.4.) and the average U-Pb age 182.8 ± 0.6 Ma of the main Karoo Basin sills is based on Svensen et al. (2012), Sell et al. (2014), Burgess et al. (2015), and Greber et al., 2020. The vertical bands P1–P4 indicate the previously proposed early, main, late, and waning phases of magmatism (Moulin et al., 2017). The other age data are from Jourdan et al. (2004, 2005, 2006, 2007b,c, 2008), Jones et al. (2001), Le Gall et al., (2002); Zhang et al. (2003), Mänttari (2008), Luttinen et al. (2015), Moulin et al. (2017), Luttinen (2021), Greber et al. (2020); Romu (2019), and Vuori (2004; Supplementary Data S5). The $^{40}\text{Ar}/^{39}\text{Ar}$ ages are shown relative to the K-decay constants of Renne et al. (2011). Age error bars correspond to 2σ .

The chronological data exhibit a wide spread of ages. Generalizing, the ages define a negatively skewed and spiked probability density distribution pattern around the main peak between ~ 182 and ~ 183 Ma (Supplementary Data S2). Overall,

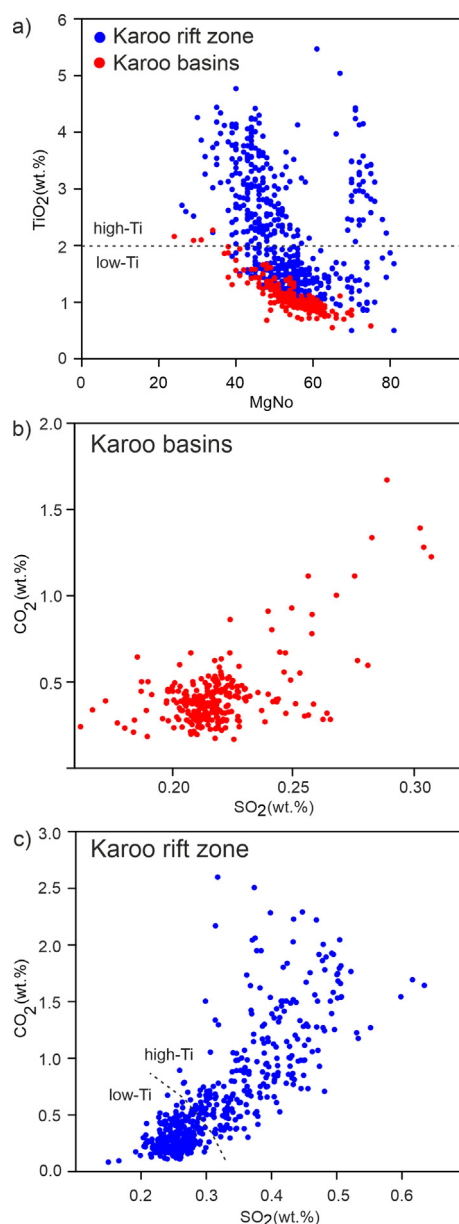


Fig. 6. Variations in Mg-number, TiO_2 , SO_2 , and CO_2 in Karoo basin and rift zone tholeiites. In a) the Mg-number of Karoo tholeiites is cation ratio $100 \cdot \text{MgO} / (\text{MgO} + 0.9\text{FeO}_{\text{total}})$ and the low-Ti vs. high-Ti boundary is after Jourdan et al. (2007a). The contents of SO_2 and CO_2 in b) Karoo basin low-Ti tholeiites and c) Karoo rift zone low-Ti and high-Ti tholeiites are calculated on the basis of TiO_2 , $\text{FeO}_{\text{total}}$, and Nb contents using the equations of Thordarson et al. (2003) and LeVoyer et al. (2017). Geochemical data for Karoo LIP ($n = 819$) are from the compilation of Luttinen (2018).

the maxima at ~ 189 Ma, ~ 183 Ma, ~ 181 Ma, ~ 179 Ma, and ~ 177 Ma broadly correspond to the periodicity (phases 1–4) recently proposed by Moulin et al. (2017). Given that the maxima at ~ 181 Ma, 179 Ma, and ~ 177 Ma represent individual high-precision U-Pb dates (Sell et al., 2014; Greber et al., 2020), the purported late phase (P3) and waning phase (P4) cannot be readily distinguished from the main phase (P2). Separate examination of the U-Pb dataset highlights the clustering of the ages at ~ 183 – 182 Ma on one hand, and the wide scatter of the high-precision ages on the other hand (Supplementary Data S2). In comparison, the $^{40}\text{Ar}/^{39}\text{Ar}$ ages define a normally distributed pattern around a peak at 182 – 181 Ma. Bearing in mind the geochemical provinciality of the Karoo LIP (Fig. 1; Luttinen, 2018), we focus

our discussion on the chronology of magmatic activity within the large Karoo basins (main Karoo Basin, Kalahari Basin) and the Karoo rift zone (African and Antarctic rifted margins, Okavango dike swarm, Lower Zambezi) (Figs. 1 and 5).

5.4.1. Timing of magmatism in the Karoo basins

The age probability distribution suggest magmatism in the Karoo basins mainly took place at ~ 183 – 182 Ma (Fig. 5). Moulin et al. (2017), however, argued for a distinctive early phase (P1) of Karoo magmatism on the basis of a single 190 ± 2 Ma $^{40}\text{Ar}/^{39}\text{Ar}$ age for a Moshesh's Ford low-Ti lava unit at the base of the Barkly East Formation, Lesotho (Fig. 5). Other examples of early phase magmatism have not been reported from the Karoo basins, but the presently available chronological data permit coeval emplacement of some sills in the main Karoo Basin and indicate contemporaneous magmatism in the Karoo rift zone (Fig. 5; section 5.4.2.).

High-precision U-Pb ID-TIMS single grain ages indicate emplacement of dolerite sills across the main Karoo Basin between 183.4 ± 0.2 Ma and 182.3 ± 0.6 Ma, possibly within <0.5 Ma at ~ 183 Ma (Svensen et al., 2012; Sell et al., 2014; Burgess et al., 2015; Greber et al., 2020) (Fig. 5). This is widely regarded to represent the main phase (P2) of Karoo magmatism. Conventional U-Pb ID-TIMS ages (183.7 ± 0.6 Ma and 182.5 ± 0.4 Ma; Encarnacion et al., 1996; Svensen et al., 2007) have a similar range, and while the $^{40}\text{Ar}/^{39}\text{Ar}$ ages for the sills (186 ± 2 Ma to 178 ± 1 Ma; Jourdan et al., 2008) show a wider spread, they mainly overlap within error with the U-Pb data (Fig. 5). The preferred 183.3 ± 0.7 Ma (average of 5; Jourdan et al., 2007c) and 181.9 ± 1.0 Ma (average of 3; Moulin et al., 2017) average $^{40}\text{Ar}/^{39}\text{Ar}$ ages of the extrusive Lesotho Formation support emplacement of the main Karoo Basin low-Ti tholeiitic lavas during this time (Fig. 5). While ~ 183 Ma $^{40}\text{Ar}/^{39}\text{Ar}$ ages are also widespread in the Kalahari Basin, the $^{40}\text{Ar}/^{39}\text{Ar}$ age data for the 800-m-thick Shadi-Shadi low-Ti basalt succession in the southeastern part of the Kalahari Basin are indicative of eruption mainly at 180.3 ± 0.5 Ma (average of 8; Jourdan et al., 2005). The young ages from the Kalahari Basin, and perhaps the single ~ 178 Ma age from the main Karoo Basin (Fig. 6), thus indicate generation of significant volumes of low-Ti tholeiites in parts of the Karoo basins during the late phase (P3) of magmatism (Fig. 5). The widespread occurrence of ~ 183 – 182 Ma capping high-Ti basalts across the Kalahari Basin (Fig. 5; section 5.4.2.; Jourdan et al., 2007a) suggests, however, that eruptions of late phase low-Ti lavas in the Karoo basins may have been largely limited to the vicinity of the Shadi-Shadi locality.

5.4.2. Timing of magmatism in the rift zone

The age probability distribution suggest magmatism in the Karoo rift zone was periodic (Fig. 5). The $^{40}\text{Ar}/^{39}\text{Ar}$ ages of 189 ± 2 Ma to 186 ± 2 Ma for low-Ti and high-Ti dikes in Vestfjella, the Dronning Maud Land subprovince (Luttinen et al., 2015), and our 188.4 ± 0.9 Ma age for rhyolite T035 and the 190 ± 2 Ma zircons in tuff T037 in Lower Zambezi, and probably the ~ 186 Ma U-poor zircon core in granite KBM6 from Vestfjella record onset of Karoo rift zone magmatism during the early phase (P1) (Fig. 5). Broadly similar $^{40}\text{Ar}/^{39}\text{Ar}$ ages have been reported elsewhere in the Dronning Maud Land subprovince, but they do not fulfill the criteria of reliable magma crystallization ages (e.g. Riley et al., 2005, 2009; Curtis et al., 2008) and are excluded from our compiled data. Bearing in mind the textural evidence of bimodality in the silicic rocks of Lower Zambezi (Manninen et al., 2008), our new ages indicate the region of early phase (P1) mantle and crustal melting extended across the entire length of the Karoo rift zone.

The ages for rift zone magmatism peak between ~ 184 Ma and 178 Ma, with narrow spikes at ~ 181 Ma, ~ 179 Ma, and ~ 177 Ma representing sparse high-precision U-Pb data (Sell et al., 2014; Greber et al., 2020) (Fig. 5). Generalizing, relatively few rift zone

ages correlate with the main phase (P2). However, the 182 ± 1 Ma U-Pb ages of two gabbro dikes from Vestfjella (ID-TIMS; Luttinen et al., 2015) and the 181.7 ± 1.0 Ma age of the Lupata tuff D005B are indistinguishable from the main phase. Furthermore, the $^{40}\text{Ar}/^{39}\text{Ar}$ data indicate that several high-Ti basalts and dikes from the Tuli Basin and some of the high-Ti dikes of the North Lebombo swarm are likely coeval with the main phase (Fig. 5). Generation of high-Ti magmas during the main phase is also recorded by the high-Ti capping basalt unit atop of a thick succession of low-Ti basalts in the Kalahari Basin (Jourdan et al., 2007a) (Fig. 5). These lavas were probably fed by the coeval first intrusive stages of the high-Ti Okavango dike swarm.

The giant Okavango dike swarm is currently the best-dated major structural component of the rift zone; the preferred 181 ± 1 Ma emplacement age of its high-Ti dikes (Jourdan et al., 2007c) is based on fifteen $^{40}\text{Ar}/^{39}\text{Ar}$ ages (Le Gall et al., 2002; Jourdan et al., 2004, 2005). Evaluation of the $^{40}\text{Ar}/^{39}\text{Ar}$ data reveals that the ages of the high-Ti tholeiitic Batoka basalts (Jones et al., 2001) and Kirwanveggen dikes (Zhang et al., 2003) as well as the low-Ti tholeiitic Utpostane layered intrusion (average of five ages; Zhang et al., 2003) and Sembberget basalts (Luttinen, 2021) are indistinguishable from the preferred age of the Okavango dikes at 181 ± 1 Ma (Fig. 5), which indicates a notably widespread pulse of mafic late phase (P3) magmatism in the rift zone. The high-Ti Batoka basalts occur outside of the main rift structure (Fig. 1), but they can be linked to the Okavango dike swarm on the basis of similar high-Ti compositions (Jones et al., 2001; Jourdan et al., 2007a) and the WNW magma flow directions in the dike swarm (Hastie et al., 2014). In Vestfjella, a U-Pb ID-TIMS zircon age of 179.9 ± 0.6 Ma from the Marginal Zone of the Utpostane layered intrusion ($^{206}\text{Pb}/^{238}\text{U}$ age recalculated from Vuori, 2004; Supplementary Data S5) is marginally younger than the 181.2 ± 0.5 Ma $^{40}\text{Ar}/^{39}\text{Ar}$ age of the intrusion interior (Zhang et al., 2003). This may relate to long-lived evolution of the > 3 -km-thick magma body, or possible Pb-loss from the notably U-rich zircons ($>5,000$ ppm). These observations and the predominance of ~ 181 – 179 Ma ages in the Tuli Basin and North Lebombo support correlation of the mafic volcanic and intrusive rift zone rocks mainly with the late phase (P3).

The 181.7 ± 1.0 Ma to 178 ± 2 Ma ages of the Lupata, Moatize-Luia, and Mbuluzi rhyolites add on to evidence of widespread silicic rift zone magmatism. These ages overlap with the 181.3 ± 0.2 Ma to 179.3 ± 0.2 Ma U-Pb ID-TIMS and $^{40}\text{Ar}/^{39}\text{Ar}$ age range of the voluminous Lebombo rhyolites (Jourdan et al., 2007b; Sell et al., 2014; Greber et al., 2020). This result is important for two reasons. First, it shows that the eruptions of the bimodal volcanic successions of Lower Zambezi and the Movene Formation, Lebombo monocline (Fig. 1), were associated with the main (P2) and late phases (P3) of Karoo magmatism (see section 5.3.). Second, it indicates penecontemporaneous emplacement of silicic magmas across the entire length of the rift zone. This is further supported by the 181.2 ± 0.8 Ma and 179.9 ± 0.9 Ma ID-TIMS ages for a cross-cutting granophyre dike in the Utpostane layered intrusion, Vestfjella ($^{206}\text{Pb}/^{238}\text{U}$ ages recalculated from Vuori, 2004; Supplementary Data S5) (Figs. 1 and 5).

The waning phase (P4) of Karoo-related magmatism is limited to the Karoo rift zone and has been previously recognized on the basis of 175.5 ± 0.7 Ma to 174 ± 2 Ma $^{40}\text{Ar}/^{39}\text{Ar}$ ages of the youngest Lebombo dolerites, including the Rooi Rand dikes (Jourdan et al., 2007b), and the ~ 178 Ma and ~ 176 Ma $^{40}\text{Ar}/^{39}\text{Ar}$ (hornblende and biotite; Jourdan et al., 2007b) and $176.84 \pm 0.06/0.2$ Ma U-Pb ID-TIMS (Greber et al., 2020) ages for silicic intrusive plugs in the Mwenezi area (Fig. 5). We consider the 172 ± 2 Ma Sica Beds rhyolite (23192A) and possibly the 165.0 ± 0.9 Ma Vestfjella granite (KBM6) to represent the waning stage. The $^{40}\text{Ar}/^{39}\text{Ar}$ chronology of the Antarctic rifted margin provides further evidence of waning

magmatic and tectonic activity, i.e. the ~ 162 Ma emplacement of lamproite dikes (phlogopite ages, Luttinen et al., 2002), ~ 173 – 154 Ma alteration of dolerite dikes (plagioclase alteration plateau ages, Luttinen et al., 2015), and ~ 154 – 142 Ma amygdale mineralization (microcline ages, Zhang et al., 2003). We point out, however, that it is difficult to define whether some of the youngest events were directly associated with the same geodynamic process that produced the Karoo province.

5.5. Implications of chronology for the origin and environmental impact of the Karoo LIP

Igneous rocks related to the Karoo basins and Karoo rift zone show contrasting geochemical characteristics (e.g. Duncan et al., 1984; Jourdan et al., 2007a; Luttinen, 2018). Consequently, the periodicity of magmatism inferred from the age data has important implications for the origin and environmental impact of the Karoo LIP. Overall, the chronological and geochemical data on the least-contaminated rock types point to tapping of depleted upper mantle during the early phase in the rift zone (e.g. Heinonen et al., 2010b; Luttinen et al., 2015) and different kinds of primitive and enriched lithospheric mantle or plume sources during the main phase magmatism in the Karoo basins and the late phase magmatism in the rift zone (Ellam et al., 1992; Sweeney et al., 1994; Ellam, 2006; Jourdan et al., 2007a; Kamenetsky et al., 2017; Howarth and Harris, 2017; Luttinen, 2018; Turunen et al., 2019; Ashwal et al., 2021). Here we focus on the implications of compositional variability in the different magmatic phases for the environmental impact of the Karoo LIP.

The formation of LIPs has been associated with major environmental crises and mass extinctions (e.g. Ernst and Youbi, 2017; Kasbohm et al., 2021) and the rapid emplacement of the main Karoo Basin low-Ti tholeiites correlates with the Pliensbachian-Toarcian extinction event at ~ 183 Ma (e.g. Svensen et al., 2007, 2012). Judging from the dispersion of reliable age data (Fig. 5), it seems possible that the other phases of magmatism could also have been linked to recurrent Pliensbachian and Toarcian extinction events dated at ~ 186 Ma, ~ 184 Ma, ~ 183 Ma, ~ 182 – 181 Ma, ~ 181 – 180 Ma, and ~ 179 – 178 Ma (Caruthers et al., 2013). Degassing of volatiles into atmosphere has been recognized as the main culprit of global climate change and biosphere collapse during LIP magmatism and the impact of volcanic volatiles depends on the contents, compositions, fluxes of the released gases and their atmospheric circulation (e.g. Self et al., 2005). These are mainly controlled by the mantle sources, emplacement mechanisms, and volumes of the magmas in addition to the duration, rate, and style of eruptions, and the interactions between magmas and volatile-rich sedimentary rocks.

In the Karoo LIP, the low-Ti tholeiitic suite of the Karoo basins and the low-Ti to high-Ti tholeiitic suite of the Karoo rift zone (Fig. 6) represent of two compositionally, geographically, and chronologically distinct parts the degassed volcanic edifice (Figs. 1 and 5; Luttinen, 2018).

Here we evaluate the fluxes of SO_2 and CO_2 from these Karoo subsystems. In the absence of direct measurements, we have estimated the mantle-derived volatile contents in undegassed mafic magmas using the compilation of geochemical data in Luttinen (2018) (Fig. 6). Based on the Thordarson et al. (2003) equation S (ppm) = $516 + 5806 \times \text{TiO}_2/\text{FeO}$ t and the calibration of LeVoyer et al. (2017) for the CO_2/Nb ($=557 \pm 79$) proxy, the undegassed SO_2 and CO_2 contents of the low-Ti tholeiitic magmas that were emplaced within the Karoo basins and the Karoo rift zone were relatively low (0.20–0.26 wt% and 0.2–0.5 wt%, respectively). In comparison, the undegassed SO_2 and CO_2 contents of the high-Ti tholeiites associated with the rift zone were roughly twice as high (mainly 0.30–0.50 wt% and 0.5–1.5 wt%, respectively). It is more

difficult to constrain the original volume of the rocks that underwent degassing, but the total magmatic volume of the Karoo LIP has been estimated to be over 10 million km^3 and the size of the volcanic edifice may have been up to 5 million km^3 (White, 1997). Presently, the exposures of Karoo basin low-Ti tholeiites occur over an area of $\sim 500,000$ km^2 (Smith, 1990; Jourdan et al., 2007a) and, judging from the tight Gondwana reconstruction in Fig. 1, the area of the main rift zone and the associated Okavango dike swarm and related lavas was of the same order. The preserved maximum thickness of the mafic lava pile is ~ 1.5 km in the Karoo basins (Marsh et al., 1997; Jourdan et al., 2007a) and up to 5 km in the rift zone (Klausen, 2009; Luttinen, 2021). Based on these constraints, we conclude that the erupted volume in the Karoo rift zone may have been broadly similar to or even larger than in the Karoo basins. To estimate the scale of magmatic degassing in the Karoo LIP, we assume the eruptive volumes of the Karoo basin lavas and the Karoo rift zone lavas were similar and together comprised a total of 2.5 million km^3 . On the basis of the volcanic stratigraphy of the Lebombo monocline (Sweeney et al., 1994), we further approximate that the volume ratio of low-Ti relative to high-Ti tholeiites in the rift zone was 1:1 or less. Using average density of 2.8 g/cm^3 for the mafic rocks and 70–80% degassing efficiency of the magmas (cf. Thordarson et al., 1996), these estimates indicate that the release of SO_2 from mantle into the atmosphere due to degassing was ~ 4.9 – 7.3 Tt in the Karoo basins and ~ 6.1 – 10.6 Tt in the Karoo rift zone. The corresponding values for CO_2 are ~ 4.9 – 14.0 Tt and 8.6–28.0 Tt, respectively. In comparison, the release of magmatic SO_2 in the ~ 3 M km^3 Siberian Traps LIP has been estimated as 12.6–15.6 Tt on the basis of volatile analyses from melt inclusions (Black et al., 2012), which suggests to us that our values for the mafic Karoo magmatism are realistic.

In the case of voluminous silicic rift zone magmatism, the metaluminous to peraluminous compositions of the Lebombo and Lower Zambezi rhyolites (Miller and Harris, 2007; Melluso et al., 2008; Manninen et al., 2008) are suggestive of low SO_2 (~ 200 ppm; Scaillet and Macdonald, 2006) and CO_2 contents (< 500 ppm; Lowenstern and Hurwitz, 2008) in the undegassed silicic magmas. Using these values and average density of 1.22 g/cm^3 for the silicic rocks (ignimbrite from Self et al., 2004), we obtain a potential release of 7.3 Gt of SO_2 and < 18.3 Gt of CO_2 just from the estimated 30,000 km^3 minimum volume of Lebombo silicic rocks (Cleverly et al., 1984). Taking into account the occurrence of silicic rocks in the Tuli, Lower Zambezi, and Dronning Maud Land parts of the rift zone, we regard that the original volumes of silicic volcanic rocks and the amounts of released volatiles were probably up to two times larger.

Our calculations suggest that the overall volumes of magmatic degassing in the Karoo basins and in the Karoo rift zone were broadly similar. Our modelling does not take into account the volatile contribution from assimilation of crustal rocks and 'cryptic' degassing of shallow intrusions (Armstrong McKay et al., 2014), but we regard the influence of these processes was uniform across the Karoo LIP (e.g. Luttinen, 2018). The role of volatiles liberated from the crustal wall-rocks of the intrusions by contact metamorphism presents a critical unknown in the comparison of volatile fluxes in the Karoo basins and the Karoo rift zone (e.g. McElwain et al., 2005). Svensen et al. (2007) proposed potential release of 27 Tt of CO_2 from the sedimentary wall-rocks of the low-Ti sills of the main Karoo Basin. Carbon-bearing sedimentary rocks also occur in the rift zone (e.g. Hjelle and Winsnes, 1972; Bordy and Prevec, 2015), but their limited exposure renders estimation of the possible sedimentary CO_2 reservoirs in the rift zone unfeasible.

The environmental impact of volatiles is highly dependent on the overall duration of magmatism and the eruption rates and styles of individual volcanic units which control the atmospheric circulation of the volatiles (e.g. Self et al., 2005). We consider that

the greatest part of Karoo LIP was formed during the main and late phases of magmatism (Fig. 5) and we focus our discussion on them.

The chronological data indicate that the low-Ti tholeiites in the Karoo basins were mostly rapidly emplaced during the main phase of magmatism (Svensen et al., 2012), but the volcanic pile of the main Karoo Basin is composed almost entirely of compound flow fields of braided-type and tabular pahoehoe (Jay et al., 2018). This indicates slow effusion rates (Single and Jerram 2004) and release of volcanic gas into lower atmosphere mainly from lava flow surface (Self et al., 2005), which would have limited the circulation of volatiles and their environmental impacts considerably.

In the case of the Karoo rift zone, we consider that the clustering of the ages of widespread high-Ti and low-Ti tholeiites at 181 ± 1 Ma (Fig. 5) implies rapid formation of the majority of the lavas and intrusions during the late phase. Moreover, detailed volcanic stratigraphy indicates that the late phase low-Ti lava successions in Antarctica are typically composed of over 20 m thick pahoehoe sheets (Harris et al., 1990; Luttinen et al., 2010; Luttinen, 2021). Many of these lava units have rubbly flow top breccias indicative of very high eruption rates capable of high fire fountaining and efficient transport of gases into the atmosphere (Self et al. 1998; Harris and Rowland 2009; Keszthelyi et al. 2006). While the estimated total volume of SO_2 and CO_2 release from silicic magmas pales in comparison with the likely volatile release from the mafic magmas, the main body of the silicic rocks was emplaced within a relatively short period as several large Plinian or Ultraplinian eruptions (Troch et al., 2020), which facilitated efficient transport of gases into the upper atmosphere (Self et al. 1998; Harris and Rowland 2009; Keszthelyi et al. 2006).

On the basis of the low volatile contents and eruption rates indicated for the main phase low-Ti magmatism, we concur with Svensen et al. (2007) in that explosive release of sediment-derived gases recorded by the abundant breccia pipes associated with sills in the main Karoo Basin, and probably in the coeval Ferrar LIP (e.g. McElwain et al., 2005), may have been the key trigger of the Toarcian-Pliensbachian global biosphere crisis. We emphasize that the Karoo rift zone magmas probably also released high amounts of volatiles into atmosphere. The largest volume of rift zone magmas appears to have been related to the late phase of igneous activity that was typified by volatile-rich high-Ti magmatism and, at least occasionally, high eruption rates capable of efficient degassing. Combined with repeated explosive release of volatiles from silicic eruptions, the late phase mafic magmatism in the Karoo rift zone provides a plausible cause for 182–178 Ma extinction events (Caruthers et al., 2013). Finally, the high extinction rates prior to the main phase (Caruthers et al., 2013) implies to us that the widespread > 185 Ma early phase Karoo magmatism may have contributed to Pliensbachian extinctions and may well represent a larger portion of the Karoo LIP than suggested by the bedrock exposures and presently available chronological data.

6. Conclusions

Our 190 ± 2 Ma, 188.4 ± 0.9 Ma, 181.7 ± 1.0 Ma, 180 ± 3 Ma, 178 ± 2 Ma and 172 ± 2 Ma U-Pb ages and Lu-Hf isotopic data on zircons in silicic rocks support episodic and long-lived magmatism in the main rift zone of the Karoo LIP. Inherited 2722–381 Ma zircons are present in many samples and most of the Jurassic zircons have negative initial ϵ_{Hf} values suggestive of predominant magma sources in the crustal basement.

The emplacement ages cannot be precisely defined due to relatively low Pb contents, limitations of the dating method, and the presumably complex and multistage evolution of the silicic intrusive and volcanic rocks. Nevertheless, the U-Pb ages make a strong case for melting of crust at ~ 190 –186 Ma, and, by inference, they

support previous $^{40}\text{Ar}/^{39}\text{Ar}$ evidence for emplacement of coeval mantle-sourced magmas during an early phase of Karoo LIP magmatism (Luttinen et al., 2015; Moulin et al., 2017).

Our results also add on to evidence of widespread bimodal rift zone magmatism in the period 182–178 Ma and correlate the Movene Formation and Lower Zambezi successions with the late phase. The age ranges of Hf isotopically uniform zircons in several samples point to formation of long-lived ~ 190 –180 Ma magma transport and storage systems in the Lower Zambezi.

In the Karoo LIP, the geographical distribution of different ages is generally compatible with shifting of the locus of magmatic activity from the main Karoo Basin and Kalahari Basin to the rift zone during the late phase. However, the sparsity of age data for the African and Antarctic rifted margins still constitutes a critical uncertainty in the geochronology of the Karoo.

We calculate from geochemical data that the mafic main phase magmas were relatively poor in CO_2 and SO_2 and note that the lava stacking patterns point to low eruption rates, which supports degassing of sedimentary wall-rocks of intrusions as the main trigger of coeval Pliensbachian-Toarcian extinction as suggested by Svensen et al. (2007). In contrast, the mafic late phase magmas were rich in CO_2 and SO_2 and at least some of the lavas suggest high eruption rates. We propose that the Karoo rift zone was typified by efficient degassing from widespread mafic magmatism and explosive eruption of > 30,000 km^3 of silicic magmas at ~ 182 –178 Ma, which associates the late phase magmatism with contemporaneous global biosphere crises (Caruthers et al., 2013).

The compositional diversity of early, main, and late phase magmas attests to the fact that the Karoo LIP is a profoundly complex system and models that advocate single sources or contemporaneous magma emplacement for the widespread igneous rocks are unwarranted and oversimplified. Along with further dating and geochemical research, detailed mapping of lava stacking properties and direct measurements of magmatic volatiles in different sub-provinces will be required for quantitative assessment of the origin, evolution, and environmental impacts of Karoo magmatism.

CRediT authorship contribution statement

Arto Luttinen: Writing – original draft, Conceptualization, Investigation, Funding acquisition, Supervision, Visualization, Resources, Project administration. **Matti Kurhila:** Formal analysis, Investigation, Writing – review & editing. **Riina Puttonen:** Investigation, Writing – review & editing. **Martin Whitehouse:** Methodology, Supervision, Validation, Writing – review & editing, Software, Resources, Data curation. **Tom Andersen:** Methodology, Supervision, Validation, Writing – review & editing, Software, Resources, Data curation.

Declaration of Competing Interest

The authors declare that they have no known competing financial interests or personal relationships that could have appeared to influence the work reported in this paper.

Acknowledgments

We thank Siri Simonsen for technical support and Magnus Kristoffersen for assistance with data handling in the Lu-Hf isotopic analyses, acknowledge Jussi Heinonen, António Alfaca, Estêvão Sumburane, and Teofilo Gove, and the Finnarp logistics for field-assistance, and are grateful to Saku Vuori for the permission to include unpublished ID-TIMS data from his PhD thesis in [Supplementary Data S5](#). Comments from reviewers João Orestes S. Santos and Richard Ernst improved the paper. The feedback from

Fred Jourdan, Lars Eivind Augland, and Kieran Iles on an earlier version of the manuscript were helpful. This is Nordsim contribution #710. This work was supported by the Academy of Finland [grant 305663].

Appendix A. Supplementary data

Supplementary data to this article can be found online at <https://doi.org/10.1016/j.gr.2022.03.005>.

References

- Allen, A.R., 1991. The tectonic and metamorphic evolution of H.U. Sverdrupfjella, western Dronning Maud Land, Antarctica. In: Thomson, M.R.A., Thomson, J.W. (Eds.), *Geological Evolution of Antarctica*. Cambridge Univ. Press, 53–60.
- Armstrong McKay, D.I., Tyrrell, T., Wilson, P.A., Foster, G.L., 2014. Estimating the impact of the cryptic degassing of Large Igneous Provinces: A mid-Miocene case-study. *Earth Planet. Sci. Lett.* 403, 254–262. <https://doi.org/10.1016/j.epsl.2014.06.040>.
- Ashwal, L.D., Ziegler, A., Glynn, S., Truebody, T., Bolhar, R., 2021. Sr-enriched glassy picrites from the Karoo Large Igneous Province are evolved, not primitive magmatic rocks. *Geochem. Geophys. Geosyst.* 22 (4). <https://doi.org/10.1029/2020GC009561>.
- Barton, C.M., Carney, J.N., Crow, M.J., Dunkey, P.N., Si-mango, S., Evans, J.A., 1991. The geology of the country around Rushinga and Nyamapanda. *Zimbabwe Geol. Surv. Bull.* 92, 220 p.
- Black, B.A., Elkins-Tanton, L.T., Rowe, M.C., Peate, I.U., 2012. Magnitude and consequences of volatile release from the Siberian Traps. *Earth Planet. Sci. Lett.* 317, 363–373. <https://doi.org/10.1016/j.epsl.2011.12.001>.
- Bordy, E.M., Prevec, R., 2015. Lithostratigraphy of the Emakwezini Formation (Karoo Supergroup). *South Africa. S. African J. Geol.* 118 (3), 307–310. <https://doi.org/10.2113/jgssaj.118.3.307>.
- Bouvier, A., Verwoort, J.D., Patchett, P.J., 2008. The Lu-Hf and Sm-Nd isotopic composition of CHUR: constraints from unequilibrated chondrites and implications for the bulk composition of terrestrial planets. *Earth Planet. Sci. Lett.* 273 (1–2), 48–57. <https://doi.org/10.1016/j.epsl.2008.06.010>.
- Bristow, J.W., Allsopp, H.L., Erlank, A.J., Marsh, J.S., Armstrong, R.A., 1984. Strontium isotope characterization of Karoo volcanic rocks. In: Erlank, A.J. (Ed.), *Petrogenesis of the volcanic rocks of the Karoo Province*. Geol. Soc. S. Africa Spec. Publ. 13, 295–329.
- Bryan, S.E., Ferrari, L., 2013. Large igneous provinces and silicic large igneous provinces: Progress in our understanding over the last 25 years. *Geol. Soc. Am. Bull.* 125 (7–8), 1053–1078. <https://doi.org/10.1130/B30820.1>.
- Burgess, S.D., Bowring, S.A., Fleming, T.H., Elliot, D.H., 2015. High-precision geochronology links the Ferrar large igneous province with early-Jurassic ocean anoxia and biotic crisis. *Earth Planet. Sci. Lett.* 415, 90–99. <https://doi.org/10.1016/j.epsl.2015.01.037>.
- Burke, K., Dewey, J.F., 1973. Plume-generated triple junctions: key indicators in applying plate tectonics to old rocks. *J. Geol.* 81 (4), 406–433. <https://doi.org/10.1086/627882>.
- Camp, V.E., Hanan, B.B., 2008. A plume-triggered delamination origin for the Columbia River Basalt Group. *Geosphere* 4 (3), 480–495. <https://doi.org/10.1130/GES00175.1>.
- Caruthers, A.H., Smith, P.L., Gröcke, D.R., 2013. The Pliensbachian-Toarcian (Early Jurassic) extinction, a global multi-phased event. *Palaeogeogr. Palaeoclimatol. Palaeoecol.* 386, 104–118. <https://doi.org/10.1016/j.palaeo.2013.05.010>.
- Cleverly, R.W., Betton, P.J., Bristow, J.W., 1984. Geochemistry and petrogenesis of the Lebombo rhyolites. In: Erlank, A.J. (Ed.), *Petrogenesis of the volcanic rocks of the Karoo Province*. Geol. Soc. S. Afr. Spec. Publ. 13, 171–194.
- Curtis, M.L., Riley, T.R., Owens, W.H., Leat, P.T., Duncan, R.A., 2008. The form, distribution and anisotropy of magnetic susceptibility of Jurassic dykes in HU Sverdrupfjella, Dronning Maud Land, Antarctica. Implications for dyke swarm emplacement. *J. Struct. Geol.* 30 (11), 1429–1447. <https://doi.org/10.1016/j.jsg.2008.08.004>.
- Duncan, A.R., Erlank, A.J., Marsh, J.S., 1984. Regional geochemistry of the Karoo igneous province. In: Erlank, A.J. (Ed.), *Petrogenesis of the volcanic rocks of the Karoo Province*. Geol. Soc. S. Afr. Spec. Publ. 13, 355–388.
- Eales, H.V., Marsh, J.S., Cox, K.G., 1984. The Karoo igneous province: An introduction. In: Erlank, A.J. (Ed.), *Petrogenesis of the volcanic rocks of the Karoo Province*. Geol. Soc. S. Afr. Spec. Publ. 13, 1–26.
- Eby, G.N., Roden-Tice, M., Krueger, H.L., Ewing, W., Faxon, E.H., Woolley, A.R., 1995. Geochronology and cooling history of the northern part of the Chilwa Alkaline Province, Malawi. *J. Afr. Earth Sci.* 20 (3–4), 275–288. [https://doi.org/10.1016/0899-5362\(95\)00054-W](https://doi.org/10.1016/0899-5362(95)00054-W).
- Elburg, M.A., Andersen, T., Bons, P.D., Simonsen, S.L., Weisheit, A., 2013. New constraints on Phanerozoic magmatic and hydrothermal events in the Mt Painter Province, South Australia. *Gondwana Res.* 24 (2), 700–712. <https://doi.org/10.1016/j.gr.2012.12.017>.
- Ellam, R.M., 2006. New constraints on the petrogenesis of the Nuanetsi picrite basalts from Pb and Hf isotope data. *Earth Planet. Sci. Lett.* 245 (1–2), 153–161. <https://doi.org/10.1016/j.epsl.2006.03.004>.
- Ellam, R.M., Carlson, R.W., Shirey, S.B., 1992. Evidence from Re–Os isotopes for plume–lithosphere mixing in Karoo flood basalt genesis. *Nature* 359 (6397), 718–721. <https://doi.org/10.1038/359718a0>.
- Encarnacion, J., Fleming, T.H., Elliot, D.H., Eales, H.V., 1996. Synchronous emplacement of Ferrar and Karoo dolerites and the early breakup of Gondwana. *Geology* 24, 535–538. [https://doi.org/10.1130/0091-7613\(1996\)024<0535:SEOFAK>2.3.CO;2](https://doi.org/10.1130/0091-7613(1996)024<0535:SEOFAK>2.3.CO;2).
- Ernst, R.E., Youbi, N., 2017. How Large Igneous Provinces affect global climate, sometimes cause mass extinctions, and represent natural markers in the geological record. *Palaeogeogr. Palaeoclimatol. Palaeoecol.* 478, 30–52. <https://doi.org/10.1016/j.palaeo.2017.03.014>.
- Ewing, R.C., Meldrum, A., Wang, L.M., Weber, W.J., Corrales, L.R., 2003. Radiation effects in zircon. In: Hanchar, J.M., Hoskin, P.W.O. (Eds.), *Zircon*. Rev. Min. Geochem. 53, 387–425.
- Frazer, R.E., Coleman, D.S., Mills, R.D., 2014. Zircon U–Pb geochronology of the Mount Givens Granodiorite: Implications for the genesis of large volumes of eruptible magma. *J. Geophys. Res. Solid Earth* 119 (4), 2907–2924. <https://doi.org/10.1002/2013JB010716>.
- Galerne, C.Y., Neumann, E.R., 2014. Geochemical fingerprinting and magmatic plumbing systems. In: Breiterkreuz, C., Rocchi, S. (Eds.), *Physical Geology of Shallow Magmatic Systems*. Springer, Cham, pp. 119–130. <https://doi.org/10.1007/978-3-319-14084-1>.
- Gao, Y.-Y., Li, X.-H., Griffin, W.L., O'Reilly, S.Y., Wang, Y.-F., 2014. Screening criteria for reliable U–Pb geochronology and oxygen isotope analysis in uranium-rich zircons: A case study from the Suzhou A-type granites, SE China. *Lithos* 192–195, 180–191. <https://doi.org/10.1016/j.lithos.2014.02.002>.
- Garland, F., Turner, S., Hawkesworth, C., 1996. Shifts in the source of the Paraná basalts through time. *Lithos* 37 (2–3), 223–243. [https://doi.org/10.1016/0024-4937\(95\)00038-0](https://doi.org/10.1016/0024-4937(95)00038-0).
- Grantham, G.H., Guise, P.D., Spell, T., Havenga, A., 1998. The chronology of Jurassic intrusions, HU Sverdrupfjella, Dronning Maud Land, Antarctica. *J. Afr. Earth Sci.* 27 (1), 92.
- Greber, N.D., Davies, J.H.F.L., Gaynor, S.P., Jourdan, F., Bertrand, H., Schaltegger, U., 2020. New high precision U–Pb ages and Hf isotope data from the Karoo large igneous province; implications for pulsed magmatism and early Toarcian environmental perturbations. *Results Geochem.* 1, 100005. <https://doi.org/10.1016/j.ringeo.2020.100005>.
- Griffin, W.L., Belousova, E.A., Shee, S.R., Pearson, N.J., O'Reilly, S.Y., 2004. Archean crustal evolution in the northern Yilgarn craton: U–Pb and Hf–isotope evidence from detrital zircons. *Precambrian Res.* 131 (3–4), 231–282. <https://doi.org/10.1016/j.precamres.2003.12.011>.
- Griffin, W.L., Pearson, N.J., Belousova, E., Jackson, S.E., van Achterbergh, E., O'Reilly, S.Y., Shee, S.R., 2000. The Hf isotope composition of cratonic mantle: LAM–MC–ICPMS analysis of zircon megacrysts in kimberlites. *Geochim. Cosmochim. Acta* 64 (1), 133–147. [https://doi.org/10.1016/S0016-7037\(99\)00343-9](https://doi.org/10.1016/S0016-7037(99)00343-9).
- Hargraves, R.B., Reháček, J., Hooper, P.R., 1997. Palaeomagnetism of the Karoo igneous rocks in southern Africa. *S. Afr. J. Geol.* 100, 195–212. <https://hdl.handle.net/10520/EJC-929052679>.
- Harris, C., Grantham, G.H., 1993. Geology and petrogenesis of the Straumsvola nepheline syenite complex, Dronning Maud Land, Antarctica. *Geol. Mag.* 130 (4), 513–532. <https://doi.org/10.1017/S0016756800020574>.
- Harris, A.J.L., Rowland, S.K., 2009. Effusion rate controls on lava flow length and the role of heat loss: a review. *IAVCEI Spec. Publ.* 12, 33–51. <https://doi.org/10.1144/IAVCEI002.3>.
- Harris, C., Marsh, J.S., Duncan, A.R., Erlank, A.J., 1990. The petrogenesis of the Kirwan Basalts of Dronning Maud Land, Antarctica. *J. Petrol.* 31 (2), 341–369. <https://doi.org/10.1093/petrology/31.2.341>.
- Harris, C., Johnstone, W.P., Phillips, D., 2002. Petrogenesis of the Mesozoic Sistejell syenite intrusion, Dronning Maud Land, Antarctica and surrounding low- $\delta^{18}\text{O}$ lavas. *S. Afr. J. Geol.* 105 (3), 205–226. <https://doi.org/10.2113/1050205>.
- Harris, C., le Roux, P., Cochrane, R., Martin, L., Duncan, A.R., Marsh, J.S., le Roex, A.P., Class, C., 2015. The oxygen isotope composition of Karoo and Etendeka picrites: high $\delta^{18}\text{O}$ mantle or crustal contamination? *Contrib. Mineral. Petrol.* 170 (1). <https://doi.org/10.1007/s00410-015-1164-1>.
- Hastie, W.W., Watkeys, M.K., Aubourg, C., 2014. Magma flow in dyke swarms of the Karoo LIP: Implications for the mantle plume hypothesis. *Gondwana Res.* 25 (2), 736–755. <https://doi.org/10.1016/j.gr.2013.08.010>.
- Hawkesworth, C.J., Marsh, J.S., Duncan, A.R., Erlank, A.J., Norry, M.J., 1984. The role of continental lithosphere in the generation of the Karoo volcanic rocks: evidence from combined Nd- and Sr-isotopes studies. In: Erlank, A.J. (Ed.), *Petrogenesis of the volcanic rocks of the Karoo Province*. Geol. Soc. S. Afr. Spec. Publ. 13, 341–354.
- Heinonen, A.P., Andersen, T., Rämö, O.T., 2010a. Re-evaluation of rapakivi petrogenesis: Source constraints from the Hf isotope composition of zircon in the rapakivi granites and associated mafic rocks of southern Finland. *J. Petrol.* 51, 1687–1709. <https://doi.org/10.1093/petrology/egq035>.
- Heinonen, J.S., Carlson, R.W., Luttinen, A.V., 2010b. Isotopic (Sr, Nd, Pb, and Os) composition of highly magnesian dikes of Vestfjella, western Dronning Maud Land, Antarctica: a key to the origins of the Jurassic Karoo large igneous province? *Chem. Geol.* 277 (3–4), 227–244. <https://doi.org/10.1016/j.chemgeo.2010.08.004>.
- Heinonen, J.S., Luttinen, A.V., Bohrson, W.A., 2016. Enriched continental flood basalts from depleted mantle melts: modeling the lithospheric contamination of Karoo lavas from Antarctica. *Contrib. Mineral. Petrol.* 171 (9). <http://dx.doi.org/10.1007/s00410-015-12>.

- Hjelle, A., Winsnes, T., 1972. The sedimentary and volcanic sequence of Vestfjella, Dronning Maud Land; Antarctic geology and geophysics. In: Adie, R.J. (Ed.), *Antarctica Geology and Geophysics*. Universitetsforlaget, pp. 539–547.
- Howarth, G.H., Harris, C., 2017. Discriminating between pyroxenite and peridotite sources for continental flood basalts (CFB) in southern Africa using olivine chemistry. *Earth Planet. Sci. Lett.* 475, 143–151. <https://doi.org/10.1016/j.epsl.2017.07.043>.
- Huppert, H.E., Sparks, S.J., 1988. The generation of granitic magmas by intrusion of basalt into continental crust. *J. Petrol.* 29 (3), 599–624. <https://doi.org/10.1093/ptrology/29.3.599>.
- Ivanov, A.V., Meffre, S., Thompson, J., Corfu, F., Kamenetsky, V.S., Kamenetsky, M.B., Demonterova, E.I., 2017. Timing and genesis of the Karoo-Ferrar large igneous province: New high precision U-Pb data for Tasmania confirm short duration of the major magmatic pulse. *Chem. Geol.* 455, 32–43. <https://doi.org/10.1016/j.chemgeo.2016.10.008>.
- Jay, A.E., Marsh, J.S., Fluteau, F., Courtillot, V., 2018. Emplacement of inflated Pā hoehoe flows in the Naude's Nek Pass, Lesotho remnant, Karoo continental flood basalt province: use of flow-lobe tumuli in understanding flood basalt emplacement. *Bull. Volcanol.* 80 (17). <https://doi.org/10.1007/s00445-017-1189-6>.
- Jokat, W., Boebel, T., König, M., Meyer, U., 2003. Timing and geometry of early Gondwana breakup. *J. Geophys. Res. Solid Earth* 108 (B9). <https://doi.org/10.1029/2002JB001802>.
- Jones, D.L., Duncan, R.A., Briden, J.C., Randall, D.E., MacNiocail, C., 2001. Age of the Batoka basalts, northern Zimbabwe, and the duration of Karoo Large Igneous Province magmatism. *Geochem. Geophys. Geosyst.* 2 (2), n/a–n/a. <https://doi.org/10.1029/2000GC000110>.
- Jourdan, F., Bertrand, H., Schärer, U., Blichert-Toft, J., Féraud, G., Kampunzu, A.B., 2007a. Major and trace element and Sr, Nd, Hf, and Pb isotope compositions of the Karoo large igneous province, Botswana-Zimbabwe: Lithosphere vs mantle plume contribution. *J. Petrol.* 48 (6), 1043–1077. <https://doi.org/10.1093/ptrology/egm010>.
- Jourdan, F., Féraud, G., Bertrand, H., Kampunzu, A.B., Tshoso, G., Le Gall, B., Tiercelin, J.J., Capiez, P., 2004. The Karoo triple junction questioned: evidence from Jurassic and Proterozoic $^{40}\text{Ar}/^{39}\text{Ar}$ ages and geochemistry of the giant Okavango dike swarm (Botswana). *Earth Planet. Sci. Lett.* 222, 989–1006. <https://doi.org/10.1016/j.epsl.2004.03.017>.
- Jourdan, F., Féraud, G., Bertrand, H., Kampunzu, A.B., Tshoso, G., Watkeys, M.K., Le Gall, B., 2005. The Karoo large igneous province: brevity, origin, and relation with mass extinction questioned by new $^{40}\text{Ar}/^{39}\text{Ar}$ age data. *Geology* 33, 745–748. <https://doi.org/10.1130/G21632.1>.
- Jourdan, F., Féraud, G., Bertrand, H., Watkeys, M.K., 2007b. From flood basalts to the inception of oceanization: example from the $^{40}\text{Ar}/^{39}\text{Ar}$ high-resolution picture of the Karoo large igneous province. *Geochem. Geophys. Geosyst.* 8 (2), n/a–n/a. <https://doi.org/10.1029/2006GC001392>.
- Jourdan, F., Féraud, G., Bertrand, H., Watkeys, M.K., Kampunzu, A.B., Le Gall, B., 2006. Basement control on dyke distribution in Large Igneous Provinces: case study of the Karoo triple junction. *Earth Planet. Sci. Lett.* 241 (1–2), 307–322. <https://doi.org/10.1016/j.epsl.2005.10.003>.
- Jourdan, F., Féraud, G., Bertrand, H., Watkeys, M.K., Renne, P.R., 2007c. Distinct brief major events in the Karoo large igneous province clarified by new $^{40}\text{Ar}/^{39}\text{Ar}$ ages on the Lesotho basalts. *Lithos* 98 (1–4), 195–209. <https://doi.org/10.1016/j.lithos.2007.03.002>.
- Jourdan, F., Féraud, G., Bertrand, H., Watkeys, M.K., Renne, P.R., 2008. The $^{40}\text{Ar}/^{39}\text{Ar}$ ages of the sill complex of the Karoo large igneous province: Implications for the Pliensbachian-Toarcian climate change. *Geochem. Geophys. Geosyst.* 9 (6), n/a–n/a. <https://doi.org/10.1029/2008GC001994>.
- Kamenetsky, V.S., Maas, R., Kamenetsky, M.B., Yaxley, G.M., Ehrig, K., Zellmer, G.F., Bindeman, I.N., Sobolev, A.V., Kuzmin, D.V., Ivanov, A.V., Woodhead, J., Schilling, J.-G., 2017. Multiple mantle sources of continental magmatism: Insights from “high-Ti” picrites of Karoo and other large igneous provinces. *Chem. Geol.* 455, 22–31. <https://doi.org/10.1016/j.chemgeo.2016.08.034>.
- Kasbohm, J., Schoene, B., Burgess, S., 2021. Radiometric Constraints on the Timing, Tempo, and Effects of Large Igneous Province Emplacement. In: Ernst, A.J., Dickson, A.J., Bekker, A. (Eds.), *Large Igneous Provinces: A Driver of Global Environmental and Biotic Changes*. AGU Geophys. Monogr. 255, 27–82. <https://doi.org/10.1002/9781119507444.ch2>.
- Keszthelyi, L., Self, S., Thordarson, T., 2006. Flood basalts on earth, Io and Mars. *J. Geol. Soc.* 163, 253–264. <https://doi.org/10.1144/0016-764904-503>.
- Klausen, M.B., 2009. The Lebombo monocline and associate feeder dyke swarm: Diagnostic of a successful and highly volcanic rifted margin? *Tectonophysics* 468, 42–62. <https://doi.org/10.1016/j.tecto.2008.10.012>.
- Korte, C., Hesselbo, S.P., 2011. Shallow-marine carbon- and oxygen-isotope and elemental records indicate icehouse–greenhouse cycles during the Early Jurassic. *Paleoceanography* 26, PA4219. <https://doi.org/10.1029/2011PA002160>.
- Le Gall, B., Tshoso, G., Jourdan, F., Féraud, G., Bertrand, H., Tiercelin, J.J., Kampunzu, A.B., Modisid, M.P., Dymenta, J., Maia, M., 2002. $^{40}\text{Ar}/^{39}\text{Ar}$ geochronology and structural data from the giant Okavango and related mafic dyke swarms, Karoo igneous province, northern Botswana. *Earth Planet. Sci. Lett.* 202 (3–4), 595–606. [https://doi.org/10.1016/S0012-821X\(02\)00763-X](https://doi.org/10.1016/S0012-821X(02)00763-X).
- Le Voyer, M., Kelley, K.A., Cottrell, E., Hauri, E.H., 2017. Heterogeneity in mantle carbon content from CO_2 -undersaturated basalts. *Nat. Commun.* 8 (1), 1–8. <https://doi.org/10.1038/ncomms14062>.
- Lowenstern, J.B., Hurwitz, S., 2008. Monitoring a Supervolcano in Repose: Heat and Volatile Flux at the Yellowstone Caldera. *Elements* 4 (1), 35–40.
- Ludwig, K.R., 2012. User's manual for Isoplot 3.75: A geochronological toolkit for Microsoft Excel, 75 pp. Berkeley Geochron. Cent. Spec. Publ. (5).
- Luttinen, A.V., 2018. Bilateral geochemical asymmetry in the Karoo large igneous province. *Sci. Rep.* 8, 5223. <https://doi.org/10.1038/s41598-018-23661-3>.
- Luttinen, A.V., 2021. Dronning Maud Land Jurassic volcanism. *Volcanology and petrology*. In: Smellie, J.L., Panter, K.S., Geyer, A. (Eds.), *Volcanism in Antarctica: 200 million years of subduction, rifting and continental break-up*. Geol. Soc. Lond. Mem. 55, 157–181. <https://doi.org/10.1144/M55-2018-89>.
- Luttinen, A.V., Furnes, H., 2000. Flood basalts of Vestfjella: Jurassic magmatism across an Archaean-Proterozoic lithospheric boundary in Dronning Maud Land, Antarctica. *J. Petrol.* 41 (8), 1271–1305. <https://doi.org/10.1093/ptrology/41.8.1271>.
- Luttinen, A.V., Zhang, X., Foland, K.A., 2002. 159 Ma Kjakebeinet lamproites (Dronning Maud Land, Antarctica) and their implications for Gondana breakup processes. *Geol. Mag.* 139, 525–539. <https://doi.org/10.1017/S001675680200674X>.
- Luttinen, A.V., Heinonen, J.S., Kurhila, M., Jourdan, F., Mänttäri, I., Vuori, S.K., Huhma, H., 2015. Depleted mantle-sourced CFB magmatism in the Jurassic Africa-Antarctica rift: Petrology and $^{40}\text{Ar}/^{39}\text{Ar}$ and U/Pb chronology of the Vestfjella dyke swarm, Dronning Maud Land, Antarctica. *J. Petrol.* 56, 919–952. <https://doi.org/10.1093/ptrology/egv022>.
- Luttinen, A.V., Leat, P.T., Furnes, H., 2010. Björnntane and Sembberget basalt lavas and the geochemical provinciality of Karoo magmatism in western Dronning Maud Land, Antarctica. *J. Volcanol. Geotherm. Res.* 198 (1–2), 1–18. <https://doi.org/10.1016/j.jvolgeores.2010.07.011>.
- Manninen, T., Eröla, T., Makitie, H., Vuori, S., Luttinen, A., Senvano, A., Manhiça, V., 2008. The Karoo volcanic rocks and related intrusions in southern and central Mozambique. In: Pekkala, Y., Lehto, T., Mäkitie, H. (Eds.), *GTK Consortium Geological Surveys in Mozambique 2002–2007*. Geol. Surv. Fin. Spec. Paper 48, 211–250.
- Mänttäri, I., 2008. Mesoarchaean to Lower Jurassic U-Pb and Sm-Nd ages from NW Mozambique. In: Pekkala, Y., Lehto, T., Mäkitie, H. (Eds.), *GTK Consortium Geological Surveys in Mozambique 2002–2007*. Geol. Surv. Fin. Spec. Paper 48, 81–119.
- Marsh, J.S., Hooper, P.R., Reháček, J., Duncan, R.A., 1997. Stratigraphy and age of the Karoo basalts of Lesotho and implications for correlations within the Karoo igneous province. In: Mahoney, J.J., Coffin, M.F. (Eds.), *Large Igneous Provinces: Continental, Oceanic, and Planetary Flood Volcanism*. Am. Geophys. Union, Geophys. Monogr. Ser. 100, 247–272.
- McElwain, J.C., Wade-Murphy, J., Hesselbo, S.P., 2005. Changes in carbon dioxide during an oceanic anoxic event linked to intrusion into Gondwana coals. *Nature* 435 (7041), 479–482. <https://doi.org/10.1038/nature03618>.
- Melluso, L., Cucciniello, C., Petrone, C.M., Lustrino, M., Morra, V., Tiepolo, M., Vasconcelos, L., 2008. Petrology of Karoo volcanic rocks in the southern Lebombo monocline, Mozambique. *J. Afr. Earth Sci.* 52 (4–5), 139–151. <https://doi.org/10.1016/j.jafrearsci.2008.06.002>.
- Miller, J.A., Harris, C., 2007. Petrogenesis of the Swaziland and Northern Natal rhyolites of the Lebombo rifted volcanic margin, South East Africa. *J. Petrol.* 48, 185–218. <https://doi.org/10.1093/ptrology/egl061>.
- Miller, J.S., Matzel, J.E.P., Miller, C.F., Burgess, S.D., Miller, R.B., 2007. Zircon growth and recycling during the assembly of large, composite arc plutons. *J. Volcanol. Geotherm. Res.* 167 (1–4), 282–299. <https://doi.org/10.1016/j.jvolgeores.2007.04.019>.
- Misra, S., Smith, A., Ray, D., Hastie, W.W., 2021. Geochemical evidence of mixing between A-type rhyolites and basalts from Southern Lebombo, South Africa: Implications for evolution of the Northern Karoo Igneous Province. *Geol. J.* 56 (2), 1072–1108. <https://doi.org/10.1002/gj.3970>.
- Moulin, M., Fluteau, F., Courtillot, V., Marsh, J., Delpéche, G., Quidelleur, X., Gérard, M., 2017. Eruptive history of the Karoo lava flows and their impact on early Jurassic environmental change. *J. Geophys. Res. Solid Earth* 122 (2), 738–772. <https://doi.org/10.1002/2016JB013354>.
- Neumann, E.-R., Svensen, H., Galerne, C.Y., Planke, S., 2011. Multistage evolution of dolerites in the Karoo Large Igneous Province, Central South Africa. *J. Petrol.* 52, 959–984. <https://doi.org/10.1093/ptrology/egr011>.
- Pik, R., Deniel, C., Coulon, C., Yirgu, G., Marty, B., 1999. Isotopic and trace element signatures of Ethiopian flood basalts: evidence for plume-lithosphere interactions. *Geochim. Cosmochim. Acta* 63 (15), 2263–2279. [https://doi.org/10.1016/S0016-7037\(99\)00141-6](https://doi.org/10.1016/S0016-7037(99)00141-6).
- Reeves, C.V., 1978. A failed Gondwana spreading axis in southern Africa. *Nature* 273 (5659), 222–223. <https://doi.org/10.1038/273222a0>.
- Renne, P.R., Balco, G., Ludwig, K.R., Mundil, R., Min, K., 2011. Response to the comment by W.H. Schwarz et al. on “Joint determination of ^{40}K decay constant and $^{40}\text{Ar}/^{40}\text{K}$ for the Fish Canyon sanidine standard, and improved accuracy for $^{40}\text{Ar}/^{39}\text{Ar}$ geochronology” by P.R. Renne et al. 2010: *Geochim. Cosmochim. Acta* 75, 5097–5100. <https://doi.org/10.1016/j.gca.2011.06.021>.
- Riley, T.R., Curtis, M.L., Leat, P.T., Millar, I.L., 2009. The geochemistry of Middle Jurassic dykes associated with the Straumsvola-Tvora alkaline plutons, Dronning Maud Land, Antarctica and their association with the Karoo large igneous province. *Mineral. Mag.* 73 (2), 206–226. <https://doi.org/10.1180/minmag.2009.073.2.205>.
- Riley, T.R., Leat, P.T., Curtis, M.L., Millar, I.L., Duncan, R.A., Fazel, A., 2005. Early-Middle Jurassic dolerite dykes from Western Dronning Maud Land (Antarctica): identifying mantle sources in the Karoo large igneous province. *J. Petrol.* 46 (7), 1489–1524. <https://doi.org/10.1093/ptrology/egi023>.
- Riley, T.R., Millar, I.L., Watkeys, M.K., Curtis, M.L., Leat, P.T., Klausen, M.B., Fanning, C.M., 2004. U-Pb zircon (SHRIMP) ages for the Lebombo rhyolites, South Africa:

- refining the duration of Karoo volcanism. *J. Geol. Soc.* 161 (4), 547–550. <https://doi.org/10.1144/0016-764903-181>.
- Romu, K. I., 2019. Origin of the Concealed Continental Crust of Vestfjella, Western Dronning Maud Land, Antarctica: Evidence from Xenoliths Hosted by Jurassic Lamproites. *Geol. Surv. Fin. Bull.* 409, Monograph: Academic dissertation, 106 p.
- Scaillet, B., Macdonald, R., 2006. Experimental and Thermodynamic Constraints on the Sulphur Yield of Peralkaline and Metaluminous Silicic Flood Eruptions. *J. Petrol.* 47 (7), 1413–1437. <https://doi.org/10.1093/petrology/egl016>.
- Self, S., Keszthelyi, L., Thordarson, T., 1998. The importance of pahoehoe. *Ann. Rev. Earth Planet. Sci.* 26, 81–110. <https://doi.org/10.1146/annurev.earth.26.1.81>.
- Self, S., Gertisser, R., Thordarson, T., Rampino, M.R., Wolff, J.A., 2004. Magma volume, volatile emissions, and stratospheric aerosols from the 1815 eruption of Tambora. *Geophys. Res. Lett.* 31, L20608. <https://doi.org/10.1029/2004GL020925>.
- Self, S., Thordarson, T., Widdowson, M., 2005. Gas fluxes from flood basalt eruptions. *Elements* 1 (5), 283–287. <https://doi.org/10.2113/gselements.1.5.283>.
- Sell, B., Ovtcharova, M., Guex, J., Bartolini, A., Jourdan, F., Spangenberg, J.E., Vicente, J.-C., Schaltegger, U., 2014. Evaluating the temporal link between the Karoo LIP and climatic–biologic events of the Toarcian Stage with high-precision U–Pb geochronology. *Earth Planet. Sci. Lett.* 408, 48–56. <https://doi.org/10.1016/j.epsl.2014.10.008>.
- Single, R.T., Jerram, D.A., 2004. The 3D facies architecture of flood basalt provinces and their internal heterogeneity: examples from the Palaeogene Skye Lava Field. *J. Geol. Soc.* 161 (6), 911–926. <https://doi.org/10.1144/0016-764903-136>.
- Sirevaag, H., Jacobs, J., Ksienzyk, A.K., Dunkl, I., Marschall, H.R., 2018. Extent, thickness and erosion of the Jurassic continental flood basalts of Dronning Maud Land, East Antarctica: A low-T thermochronological approach. *Gondwana Res.* 61, 222–243. <https://doi.org/10.1016/j.jgr.2018.04.017>.
- Smith, R.M.H., 1990. A review of stratigraphy and sedimentary environments of the Karoo Basin of South Africa. *J. Afr. Earth Sci.* 10 (1–2), 117–137. [https://doi.org/10.1016/0899-5362\(90\)90050-0](https://doi.org/10.1016/0899-5362(90)90050-0).
- Söderlund, U., Patchett, P.J., Vervoort, J.D., Isachsen, C.E., 2004. The ^{176}Lu decay constant determined by Lu–Hf and U–Pb isotope systematics of Precambrian mafic intrusions. *Earth and Planetary Science Letters* 219 (3–4), 311–324.
- Spencer, C.J., Kirkland, C.L., Taylor, R.J.M., 2016. Strategies towards statistically robust interpretations of in situ U–Pb zircon geochronology. *Geosci. Front.* 7 (4), 581–589. <https://doi.org/10.1016/j.gsf.2015.11.006>.
- Stacey, J.S., Kramers, J.D., 1975. Approximation of terrestrial lead isotope evolution by a two-stage model. *Earth Planet. Sci. Lett.* 26 (2), 207–221. [https://doi.org/10.1016/0012-821X\(75\)90088-6](https://doi.org/10.1016/0012-821X(75)90088-6).
- Svensen, H., Corfu, F., Polteau, S., Hammer, Ø., Planke, S., 2012. Rapid magma emplacement in the Karoo Large Igneous Province. *Earth Planet. Sci. Lett.* 325–326, 1–9. <https://doi.org/10.1016/j.epsl.2012.01.015>.
- Svensen, H., Planke, S., Chevillier, L., Malthe-Sørensen, A., Corfu, F., Jamtveit, B., 2007. Hydrothermal venting of greenhouse gases triggering Early Jurassic global warming. *Earth Planet. Sci. Lett.* 256 (3–4), 554–566. <https://doi.org/10.1016/j.epsl.2007.02.013>.
- Sweeney, R.J., Duncan, A.R., Erlank, A.J., 1994. Geochemistry and petrogenesis of central Lebombo basalts of the Karoo igneous province. *J. Petrol.* 35 (1), 95–125. <https://doi.org/10.1093/petrology/35.1.95>.
- Thordarson, T., Self, S., Miller, D.J., Larsen, G., Vilmundardóttir, E.G., 2003. Sulphur release from flood lava eruptions in the Geivötn, Grímsvötn and Katla volcanic systems. *Iceland. Geol. Soc. Lond. Spec. Publ.* 213 (1), 103–121. <https://doi.org/10.1144/GSL.SP.2003.213.01.07>.
- Thordarson, T., Self, S., Óskarsson, N., Hulsebosch, T., 1996. Sulfur, chlorine, and fluorine degassing and atmospheric loading by the 1783–1784 AD Laki (Skaftár Fires) eruption in Iceland. *Bull. Volcanol.* 58, 205–225. <https://doi.org/10.1007/s004450050136>.
- Troch, J., Ellis, B.S., Harris, C., Bachmann, O., Bindeman, I.N., 2020. Low- $\delta^{18}\text{O}$ silicic magmas on Earth: A review. *Earth-Sci. Rev.* 208, 103299. <https://doi.org/10.1016/j.earscirev.2020.103299>.
- Turunen, S.T., Luttinen, A.V., Heinonen, J.S., Jamal, D.L., 2019. Luenha picrites, Central Mozambique – Messengers from a mantle plume source of Karoo continental flood basalts? *Lithos* 346–347, 105152. <https://doi.org/10.1016/j.lithos.2019.105152>.
- Vuori, S.K., 2004. Petrogenesis of the Jurassic gabbroic intrusions of Vestfjella, Dronning Maud Land, Antarctica. Unpubl. PhD thes. Univ. Helsinki Fin.
- Vuori, S.K., Luttinen, A.V., 2003. The Jurassic gabbroic intrusions of Utpostane and Muren: insights into Karoo-related plutonism in Dronning Maud Land, Antarctica. *Antarct. Sci.* 15 (2), 283–301. <https://doi.org/10.1017/S0954102003001287>.
- Ware, B., Jourdan, F., Tohver, E., Fernandes, K.G., Chiaradia, M., 2018. Primary hydrous minerals from the Karoo LIP magmas: Evidence for a hydrated source component. *Earth Planet. Sci. Lett.* 503, 181–193. <https://doi.org/10.1016/j.epsl.2018.09.017>.
- Watkeys, M.K., 2002. Development of the Lebombo rifted volcanic margin of southeast Africa. *Geol. Soc. Am. Spec. Pap.* 362, 27–46.
- Wendt, I., Carl, C., 1991. The statistical distribution of the mean squared weighted deviation. *Chem. Geol. Isot. Geosci. Sect.* 86 (4), 275–285. [https://doi.org/10.1016/0168-9622\(91\)90010-T](https://doi.org/10.1016/0168-9622(91)90010-T).
- White, R.S., 1997. Mantle plume origin for the Karoo and Ventersdorp flood basalts. *South Africa. S. Afr. J. Geol.* 100 (4), 271–282. <https://hdl.handle.net/10520/EJC-92973aa30>.
- White, L.T., Ireland, T.R., 2012. High-uranium matrix effect in zircon and its implications for SHRIMP U–Pb age determinations. *Chem. Geol.* 306–307, 78–91. <https://doi.org/10.1016/j.chemgeo.2012.02.025>.
- Whitehouse, M.J., Kamber, B.S., 2005. Assigning dates to thin gneissic veins in high-grade metamorphic terranes: a cautionary tale from Akilia, southwest Greenland. *J. Petrol.* 46, 291–318. <https://doi.org/10.1093/petrology/egh075>.
- Whitehouse, M.J., Kamber, B.S., Moorbath, S., 1999. Age significance of U–Th–Pb zircon data from early Archaean rocks of west Greenland—a reassessment based on combined ion-microprobe and imaging studies. *Chem. Geol.* 160 (3), 201–224. [https://doi.org/10.1016/S0009-2541\(99\)00066-2](https://doi.org/10.1016/S0009-2541(99)00066-2).
- Williams, I.S., Hergt, J.M., 2000. U–Pb dating of Tasmanian jolerites: a cautionary tale of SHRIMP analysis of high-U zircon. In: Woodhead, J.D., Hergt, J.M., Noble, W.P. (Eds.), *Beyond 2000: New Frontiers in Isotope Geoscience*. Lorne, Abstract Proceedings, 185–188.
- Wiedenbeck, M., Allé, P., Corfu, F., Griffin, W.L., Meier, M., Oberli, F., Quadt, A.V., Roddick, J.C., Spiegel, W., 1995. Three natural zircon standards for U–Th–Pb, Lu–Hf, trace element and REE analyses. *Geostand. Newsl.* 19 (1), 1–23. <https://doi.org/10.1111/j.1751-908X.1995.tb00147.x>.
- Woodhead, J.D., Hergt, J.M., 2005. A preliminary appraisal of seven natural zircon reference materials for in situ Hf isotope determination. *Geostand. Geoanalytical Res.* 29 (2), 183–195. <https://doi.org/10.1111/j.1751-908X.2005.tb00891.x>.
- Zhang, X., Luttinen, A.V., Elliot, D.H., Larsson, K., Foland, K.A., 2003. Early Jurassic Gondwana breakup: The $^{40}\text{Ar}/^{39}\text{Ar}$ geochronology of Jurassic basaltic rocks from western Dronning Maud Land, Antarctica, and implications for the timing of magmatic and hydrothermal events. *J. Geophys. Res.* 108 (B9), 2449. <https://doi.org/10.1029/2001JB001070>.